Accepted Manuscript

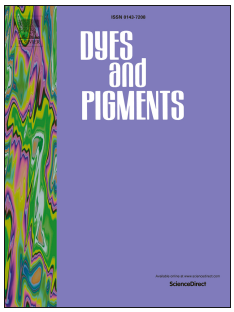

Tuning the solid-state emission of small push-pull dipolar dyes to the far-red through variation of the electron-acceptor group

Sébastien Redon, Gwenaëlle Eucat, Martin Ipuy, Erwann Jeanneau, Isabelle Gautier-Luneau, Alain Ibanez, Chantal Andraud, Yann Bretonnière

PII: S0143-7208(18)30415-7

DOI: 10.1016/j.dyepig.2018.03.049

Reference: DYPI 6634

To appear in: *Dyes and Pigments*

Received Date: 20 February 2018

Revised Date: 22 March 2018

Accepted Date: 23 March 2018

Please cite this article as: Redon Sé, Eucat Gwenaë, Ipuy M, Jeanneau E, Gautier-Luneau I, Ibanez A, Andraud C, Bretonnière Y, Tuning the solid-state emission of small push-pull dipolar dyes to the far-red through variation of the electron-acceptor group, *Dyes and Pigments* (2018), doi: 10.1016/j.dyepig.2018.03.049.

Tuning the Solid-State Emission of Small Push-pull Dipolar Dyes to the Far-red Through Variation of the Electron-acceptor Group

Sébastien Redon,[a] *Gwenaëlle Eucat,,*[a,b] *Martin Ipuy,*[a] *Erwann Jeanneau,*[c] *Isabelle Gautier-Luneau,*[b] *Alain Ibanez,*[b] *Chantal Andraud*[*,a] *and Yann Bretonnière*[*,a]

[a] Univ Lyon, ENS de Lyon, CNRS UMR 5182, Université Lyon 1, Laboratoire de Chimie, F-69342 Lyon (France).

[b] Univ. Grenoble Alpes, Institut Néel, F-38042 Grenoble (France).

CNRS, Institut Néel, F-38042 Grenoble (France).

Institute of Engineering, Univ. Grenoble Alpes

[c] Centre de Diffractométrie Henri Longchambon, Université Lyon I, 43 boulevard du 11 Novembre 1918, F-69622 Villeurbanne Cedex (France).

chantal.andraud@ens-lyon.fr / yann.bretonniere@ens-lyon.fr

RECEIVED DATE (to be automatically inserted after your manuscript is accepted if required according to the journal that you are submitting your paper to)

Abstract

Series of solid-state emitters based on the D-π-A dipolar structure and featuring various electron-donor and electron-acceptor groups were designed, and their spectroscopic properties studied. From weak

emission in dilute solutions, intense emissions in aggregated state (AIE) and in the crystalline state were obtained. Analysis in light of crystal structures obtained by X-ray diffraction revealed specific crystal packing and presence of long chain of emitting aggregates. This simple molecular engineering around the D-π-A dipolar structure provides easy access to a wide range of effective solid-state emitters allowing modulation of emission wavelengths up to the near infrared (λ_{em} reaching 735 and 768 nm for compound **2f** and **3f** bearing the strongest electron-withdrawing group).

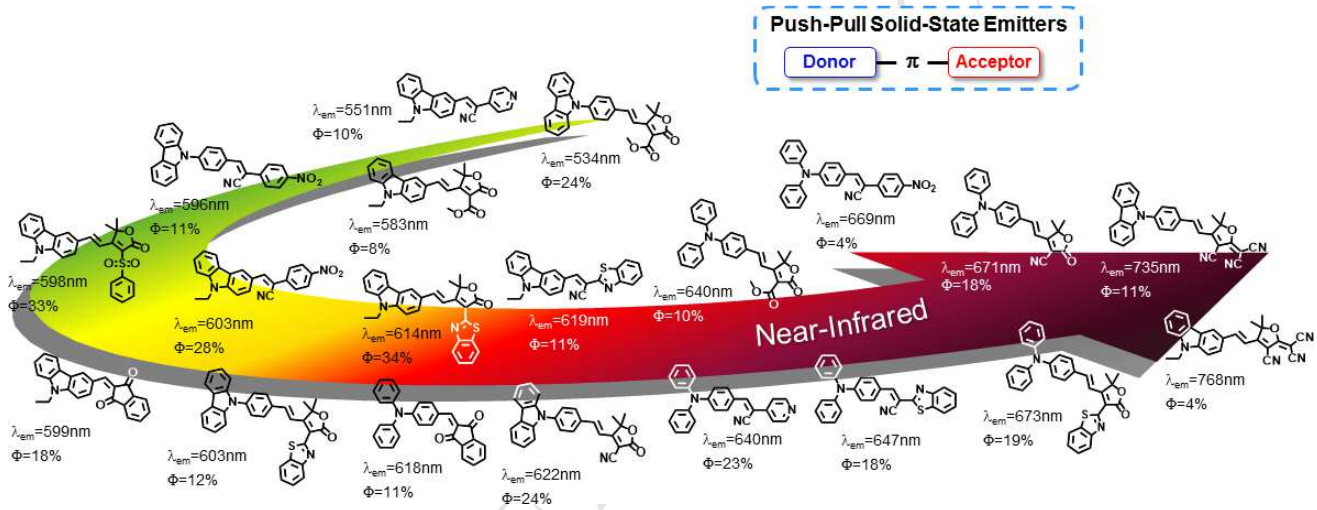

Highlights

- Library of small push-pull dipolar solid-state emitters has been obtained featuring three different electron-donor groups and various electro-acceptor groups.
- New electron-acceptor groups based on substituted 2(5*H*)-furanone rings are presented.
- Fluorescence properties in the aggregated state and in the solid-state are described, and correlated to the presence of specific aggregates in the crystal structure.
- The best dyes displayed near-infrared emission in the solid-state with emission quantum yield of 11% at λ_{em}=735 nm and 4% at λ_{em}=768 nm.

Keywords

Solid-state fluorescence; Push-pull dyes; Organic dyes; Near-infrared; Aggregation-induced emission; 2(5H)-furanone rings

1. Introduction

Engineering around organic solid-state emitters has become a thriving area of research these last few years, impelled by potential applications in the field of optoelectronics, materials and bio-imaging.[1-4] In that particular context, fluorescent organic nanocrystals or emissive organic nanoparticles based on fluorophores displaying aggregation-induced emission (AIE) properties are a promising alternative to dissolved fluorophores or to inorganic quantum dots.[5, 6] Advantages include higher absorption and higher photo-stability, combined to the infinite possibilities offered by organic synthesis to functionalize the dye and to tune the spectroscopic properties. In particular, shifting the emission wavelength towards the far-red and even the near infrared (NIR) in the first biological transparency window (λ_{em}>650 nm) is a requisite for deeper *in-vivo* imaging.[7-10] This wavelength range allows enhanced penetration depth and better contrast compared to the visible, due to lower absorption, minimized scattering and lower self-fluorescence from biological samples. However so far, good solid-state fluorophores with far-red / NIR emissions are still scarce despite increasing number of structures available and a tremendous work on AIE-active fluorophore design.[5, 11] On the one hand, interesting long wavelength solid-state emitters can be obtained by decorating red emitting dyes with the AIE-active segment, classically triphenylethene,[12-16] but also triphenylamine which also acts as potent electron-donor group.[17-21] However, this molecular engineering gives rise to rather big molecular weights and complex structures requiring sophisticated syntheses. On the other hand, recent works highlighted the interest of simple and small molecular weight *D*-π-*A* push-pull dipolar fluorophores, in which an ~~electron~~ electron-donating group *D* is connected to an electron-withdrawing group *A via* a π-conjugated bridge, for the design of efficient solid-state emitters.[22-27],[28-31],[32-39],[40],[41]

The permanent dipole moment associated with the *D-π-A* structure gives rise to strong dipole-dipole interactions that can induce specific organization and orientation of molecules in the solid-state and favors the formation of emissive aggregates. Moreover, since the fluorescence of such dipolar fluorophores is usually characterized by a large Stokes shift, red and even far-red emission wavelengths over 700 nm are accessible, providing appropriate combinations of electron-donor and acceptor groups. Association of electron-deficient 2*H*-indazoles with electron-rich heteroarenes [42] or of quinoline-malononitrile electron-withdrawing group with the electron-rich triphenylamino group [43] gives access to low molecular weight fluorophores with emission wavelengths exceeding 720 nm in the solid-state, as recently reported. Tuning of the substituents on the core skeleton also greatly influence the molecular organization in the crystal state and consequently the emission quantum yield in the solid-state, as this was illustrated in our earlier work on methoxy-substituted push-pull fluorophores bearing 2-dicyanomethylene-3-cyano-4,5,5-trimethyl-2,5-dihydrofurane (*TCF*) as electron-acceptor group.[41] Varying the number and the position of the methoxy groups have a drastic impact on the solid-state emission modulating the emission wavelength from 580 nm to 730 nm for the reddest shifted dye, while also influencing the emission efficiency. Similarly, with 2-(3,5,5-trimethylcyclohex-2-en-1-ylidene)malononitrile (*dicyanoisophorone*) as electron-accepting group and *N,N*-dialkylamino group as electron-donor, emission above 700 nm could be obtained when *J*-aggregates in the form of inclined alignment of dipoles are present in the packing resulting in sharpening of the excitation and red-shift of fluorescence.[40]

In continuation of our previous works on dipolar solid-state emitters,[40-41] we want to present here a library of push-pull fluorophores featuring 4-(*N*,*N*-diphenylamino)phenyl- (Series **1**, Chart 1), 9-ethyl-9*H*-carbazolyl- (Series **2**) and 4-(9*H*-carbazol-9-yl)- (Series **3**) as electron-donor groups and various electron-acceptor groups (**A** - **J**, Scheme 1), in particular 2(5*H*)-furanone rings with a weak electron-withdrawing group at the C*2* position (**G** - **J**). If some of these acceptor groups such as indanedione (**A**), *dicyanoisophorone* (**E**) or *TCF* (**F**) are quite commonly used in several high efficiency solid-state

emitters, [32, 38-41, 44-50] other 2(5*H*)-furanones have rarely been utilized as acceptors entities in dye design and only within the frame of non-linear optical chromophores design (acceptor group **G**).[51, 52]

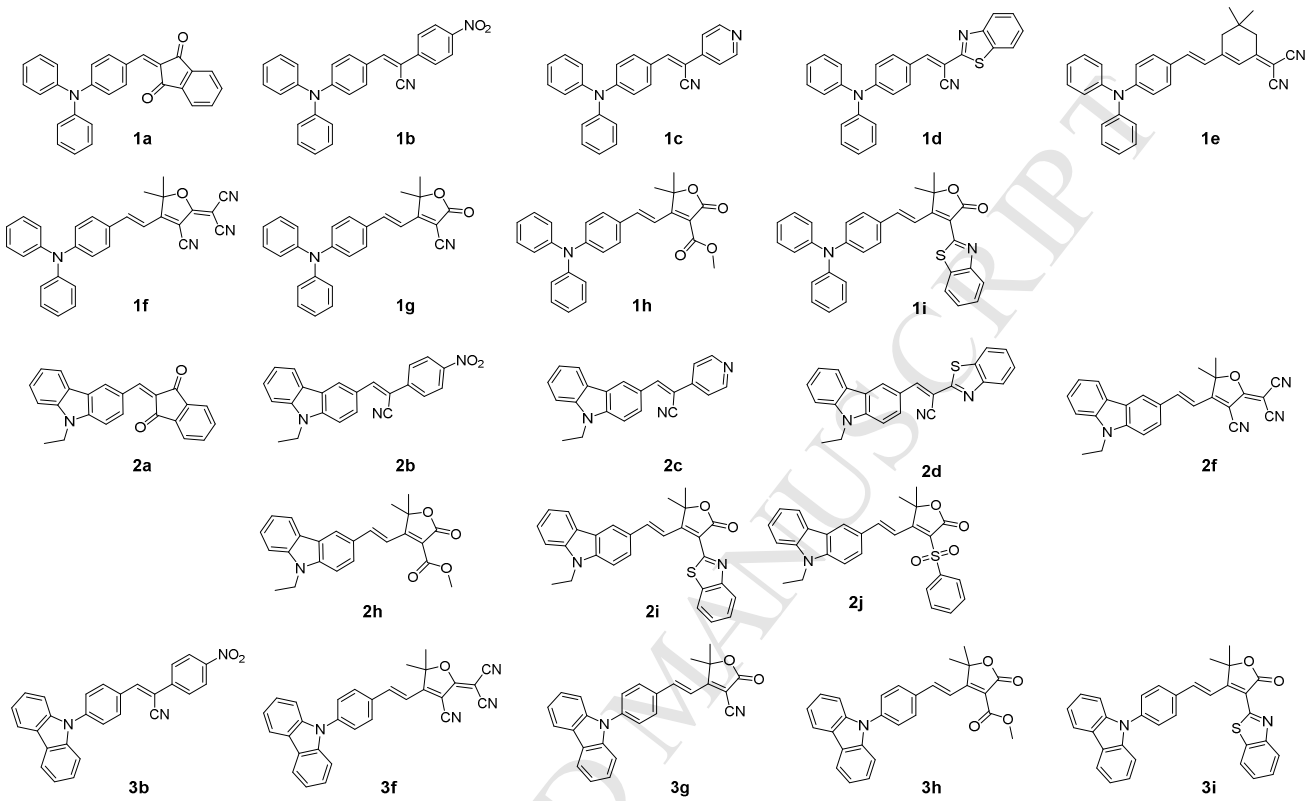

Chart 1. Structures of fluorophores **1a**-**1i**, **2a**-**2j** and **3b**-**3i**.

2. Experimental

2.1 General Information

Commercially available materials and reagent grade solvents were used as received. Microwave syntheses were conducted in 20 mL sealed tube on a Biotage Initiator 2.5 single-mode reactor using external IR temperature control. The reaction monitoring was performed by analytical thin-layer chromatography (TLC) on Merck 60 F254 precoated silica gel plate (0.2 mm thickness) with visualization using a UV lamp. Purification by column chromatography was carried out using 35-70 μm silica gel. ^{1}H and ^{13}C NMR spectra were recorded at ambient temperature on a Bruker Advance 300,

400 or 500 operating at 300.1, 400.0 or 500.0 MHz for ^{1}H and 75.0, 101.00 or 125.0 MHz for ^{13}C, respectively. Chemical shifts are reported as δ values (ppm) with reference to the residual solvent peaks. For proton, data are reported as follows: chemical shift, multiplicity (s = singlet, d = doublet, t = triplet, q = quartet, m = multiplet, b = broad), coupling constants in Hz. IR spectra were recorded on a FT/IR-4200 type A spectrometer. High-resolution mass spectrometry measurements were performed at the *Centre Commun de Spectrométrie de Masse* (UCBL, Villeurbanne, France). Melting points were recorded on a calibrated Koffler bench. Ethyl phenylsulfonylacetate,[53] compounds **1**, **E** and **1e**,[40] **3**,[54] and **F** [41] were obtained according to reported procedures. Spectroscopic data for known compounds **1a**,[55] **1b**,[56] **1c**,[57] **2a**,[39] **2b**,[56] **2c**,[58] **2f** [59] matched literature values.

2.2 Synthetic procedures and characterization data ~~for new compounds~~

2.2.1 General Protocol 1: *Knoevenagel Reaction*. Aldehyde (1 equiv.) and acceptor compound (1 equiv.) were dissolved in acetonitrile (100 mL for 14 mmol.). Piperidine (0.01 equiv.) was added and solution was stirred at the temperature indicated for the time indicated in each protocol. The solution was then concentrated under *vacuum* and the product purified by column chromatography on silica gel.

2.2.2 General Protocol 2: *Microwave Reaction*. Aldehyde (1 equiv.) and acceptor compound (1 equiv.) were dissolved in a solution of dried acetonitrile (1 mL for 1 mmol) in a microwave tube and 2 drops of piperidine were added. The tube was sealed and the mixture was heated at 110°C for 40 minutes by focused microwave irradiation under controlled temperature. After cooling to room temperature, the solvents were evaporated under *vacuum* and the product was purified by column chromatography on silica gel.

2.2.3 4,5,5'-trimethyl-2-oxo-2,5-dihydrofuran-3-carbonitrile (G). Sodium (80 mg, 3.3 mmol) was slowly added at 0°C to dry methanol (4 mL). Once everything was dissolved, 3-hydroxy-3-methyl-butan-2-one **4** (650 µL, 6.1 mmol) and ethyl cyanoacetate (1.4 mL, 13 mmol) were added at 0°C. After 12 h, the reaction was quenched by the addition of acetic acid (5 mL). The solvents were evaporated

under reduced pressure. The crude was partitioned between water (25 mL) and CH_2Cl_2 (25 mL). The organic phase was dried on Na_2SO_4, filtered and evaporated. Purification by column chromatography on silica gel eluting with ethyl acetate / cyclohexane (30/70, v/v) gave **G** as yellow solid (1.25 g, yield = 82%): m.p. 54°C; ^{1}H-NMR ($CDCl_3$, 300 MHz, δ/ppm) 1.50 (s, 6H), 2.28 (s, 3H); ^{13}C-NMR ($CDCl_3$, 101 MHz, δ/ppm) 184.8, 165.4, 110.7, 104.5, 88.3, 24.3, 13.8; IR (ν/cm^{-1}) 3448, 2239, 1764, 1650, 1288, 1080, 910.

2.2.4 Methyl 4,5,5'-trimethyl-2-oxo-2,5-dihydrofuran-3-carboxylate (H). Sodium (80 mg, 3.3 mmol) was added slowly at 0°C to dry methanol (4 mL). After full dissolution, 3-hydroxy-3-methyl-butan-2-one **4** (650 µL, 6.1 mmol) and methyl malonate (700 µL, 6.1 mmol) were added at 0°C. After 2 h, the reaction was quenched by adding a saturated aqueous NH_4Cl solution (10 mL). EtOAc (25 mL) was then added. The organic phase was separated, dried on Na_2SO_4, filtered and concentrated under reduced pressure. Purification by column chromatography on silica gel eluting with EtOAc/petroleum ether (30/70, v/v) afforded **H** (710 mg, yield = 59 %) as white solid; m.p. 65°C; ^{1}H-NMR ($CDCl_3$, 300 MHz, δ/ppm) 3.88 (s, 3H), 2.35 (s, 3H), 1.48 (s, 6H); ^{13}C-NMR ($CDCl_3$, 101 MHz, δ/ppm) 181.2, 167.2, 162.2, 118.0, 85.4, 52.1, 24.3, 13.0; IR (ν/cm^{-1}) 1760, 1711, 1350, 1280, 1191, 1174, 1043, 969, 808.

2.2.5 3-(benzo[*d*]thiazol-2-yl)-4,5,5-trimethylfuran-2(5*H*)-one (I). **G** (906 mg, 6 mmol), 2-hydroxythiophenol (640 µL, 6 mmol) and 85% aqueous phosphoric acid (3 g) were heated at 120°C for 14 h. After cooling down to room temperature, water (50 mL) was added. The mixture was carefully neutralized by slow addition of saturated aqueous K_2CO_3 (50 mL). The solution was extracted with dichloromethane three times. The combined organic layers were washed with water, dried over Na_2SO_4, filtered and evaporated to dryness to give **I**, used without further purification. Brown solid (1.41 g, yield = 91 %); m.p. 158-160°C; ^{1}H-NMR ($CDCl_3$, 300 MHz, δ/ppm) 8.07 (d, J = 8.2 Hz, 1H), 7.94 (d, J = 8.2 Hz, 1H), 7.53 (t, J = 8.2 Hz, 1H), 7.43 (t, J = 8.2 Hz, 1H), 2.68 (s, 3H), 1.59 (s, 6H); ^{13}C-NMR ($CDCl_3$, 101 MHz, δ/ppm) 172.3, 170.3, 157.9, 153.0, 135.1, 126.3, 125.6, 123.3, 121.8, 119.0, 87.0, 24.7, 13.6; IR (ν/cm^{-1}) 2173, 1644, 1497, 1055, 970, 958, 764.

2.2.6 4,5,5'-trimethyl-3-(phenylsulfonyl)furan-2(*5H*)-one (J). Sodium (70 mg, 3.04 mmol) was slowly added at 0°C to dry methanol (5 mL). After complete dissolution, 3-hydroxy-3-methyl-butan-2-one **4** (1.05 mL, 10 mmol.) and ethyl phenylsulfonylacetate (2.51 g, 11 mmol) were added at 0°C. The mixture was then heated at 50°C overnight. After cooling to room temperature, the solvent was removed under reduced atmosphere to give an oily residue. Et_2O was added to precipitate the product. The solid was filtered, washed with Et_2O and dried. Recrystallization in a mixture Et_2O/EtOAc (40 mL / 4 mL) gave compound **J** as white solid (1.5 g, 56%); m.p. 172°C; ^{1}H-NMR ($CDCl_3$, 300 MHz, δ/ppm) 8.08 (d, *J* = 7.5 Hz, 2H), 7.66 (t, *J* = 7.3 Hz, 1H), 7.56 (t, *J* = 7.2 Hz, 2H), 2.51 (s, 3H), 1.47 (s, 6H). ^{13}C-NMR ($CDCl_3$, 101 MHz, δ/ppm) 179.1, 164.7, 139.4, 134.4, 129.3, 128.8, 126.9, 86.7, 24.3, 12.6. IR (ν/cm^{-1}) 1746, 1320, 1311, 1266, 1149, 1084, 1029, 719, 685.

2.2.7 2-(4-(diphenylamino)benzylidene)-1*H*-indene-1,3(2*H*)-dione (1a). From **1** (400 mg, 1.45 mmol.) and **A** (255 mg, 1.75 mmol.) following *general protocol 1* (40°C, 18 h). Purification by chromatography (Petroleum ether, EtOAc: 9/1 v/v) afforded the title compound **1a**. Red solid (230 mg, yield = 33%); m.p. 214°C; ^{1}H-NMR (CD_2Cl_2, 400 MHz, δ/ppm) 8.41 (d, *J* = 8.8 Hz, 2H), 8.06 – 7.85 (m, 2H), 7.76 (dd, *J* = 10.7, 5.3 Hz, 3H), 7.39 (t, *J* = 7.7 Hz, 4H), 7.23 (d, *J* = 6.2 Hz, 6H), 6.99 (d, *J* = 8.8 Hz, 2H); ^{13}C-NMR (CD_2Cl_2, 101 MHz, δ/ppm) 191.3 (CO), 153.2, 146.5 (CH), 146.2, 142. 9, 140.5, 137.2 (2 x CH), 135.3 (CH), 135.12 (CH), 130.3 (4 x CH), 127.2 (4 x CH), 126.1 (2 x CH), 123.2 (CH), 123.1 (CH), 119.1 (2 x CH); IR (ν/cm^{-1}) 3062, 1680 (ν_{CO}), 1570/1542/1487, 1265, 1154; HRMS (ESI$^+$) calcd for $C_{28}H_{20}NO_2$ $[M+H]^+$: 402.1489, found: 402.1482; UV-Vis (CH_2Cl_2) λ_{max} = 485 nm (ε = 37 800 L.mol^{-1}.cm^{-1}).

2.2.8 (*Z*)-3-(4-(diphenylamino)phenyl)-2-(4-nitrophenyl)acrylonitrile (1b). From **1** (350 mg, 1.25 mmol.) and **B** (250 mg, 1.5 mmol.) following *general protocol 1* (45°C, 4 h). Purification by chromatography (CH_2Cl_2) afforded the title compound **1b**. Red solid (340 mg, yield = 33%); m.p. 145°C; ^{1}H-NMR (CD_2Cl_2, 500 MHz, δ/ppm) 8.27 (d, *J* = 8.8 Hz, 2H), 7.83 (dd, *J* = 12.6, 8.9 Hz, 4H), 7.60 (s, 1H), 7.36 (t, *J* = 7.8 Hz, 4H), 7.19 (d, *J* = 7.9 Hz, 6H), 7.03 (d, *J* = 8.8 Hz, 2H); ^{13}C NMR (125

MHz, CD_2Cl_2, δ/ppm) 151.8, 148.1, 147.0, 145.5, 142.3, 132.2 (2 x CH), 130.4 (4 x CH), 126.9 (4 x CH), 126.9 (2 x CH), 126.0, 125.7 (2 x CH), 125.0 (2 x CH), 120.6 (2 x CH), 118.8, 105.5 (CN); IR (ν/cm^{-1}) 3060, 2208 (ν_{CN}), 1572/1490/1508, 1338, 1198, 700; HRMS (ESI^+) calcd for $C_{27}H_{20}N_3O_2$ $[M+H]^+$: 418.1550, found: 418.1543; UV-Vis (CH_2Cl_2) λ_{max} = 456 nm (ε = 28 700 $L.mol^{-1}.cm^{-1}$).

2.2.9 (*Z*)-3-(4-(diphenylamino)phenyl)-2-(pyridin-4-yl)acrylonitrile (1c). From **1** (100 mg, 0.4 mmol.) and **C** (70 mg, 0.45 mmol.) following *general protocol 1* (40°C, 4 h). Purification by chromatography (CH_2Cl_2/Et_3N: 95/5 then 92/8 v/v) afforded the title compound **1c**. Orange solid (90 mg, yield = 60%); m.p. 182°C. ^{1}H-NMR (CD_2Cl_2, 500 MHz, δ/ppm) 8.62 (d, *J* = 4.8 Hz, 2H), 7.83 (d, *J* = 8.8 Hz, 4H), 7.64 (s, 1H), 7.56 – 7.46 (m, 2H), 7.35 (t, *J* = 7.8 Hz, 4H), 7.18 (t, *J* = 8.0 Hz, 6H), 7.03 (d, *J* = 8.8 Hz, 2H); ^{13}C-NMR (CD_2Cl_2, 125 MHz, δ/ppm) 151.1, 150.6 (2 x CH), 146.4, 144.4, 142.5, 131.5 (2 x CH), 129.8 (4 x CH), 126.3 (4 x CH), 125.3, 125.0 (2 x CH), 120.0 (2 x CH), 119.6 (2 x CH), 117.9, 104.6 (CN); IR (ν/cm^{-1}) 3057, 2924, 2206 (ν_{CN}), 1577/1557/1487, 1176, 756. HRMS (ESI^+) calcd for $C_{26}H_{20}N_3$ $[M+H]^+$: 374.1652, found: 374.1656; UV-Vis (CH_2Cl_2) λ_{max} = 427 nm (ε = 29 700 $L.mol^{-1}.cm^{-1}$).

2.2.10 (*E*)-2-(benzo[d]thiazol-2-yl)-3-(4-(diphenylamino)phenyl)acrylonitrile (1d). From **1** (700 mg, 2.5 mmol.) and **D** (520 mg, 3 mmol.) following *general protocol 1* (40°C, 4 h). Purification by chromatography (eluting with CH_2Cl_2) afforded the title compound **1d**. Red solid (840 mg, yield = 79%); m.p. 173°C; ^{1}H-NMR (CD_2Cl_2, 500 MHz, δ/ppm) 8.05 (s, 1H), 8.01 (d, *J* = 5.0 Hz, 1H), 7.92 – 7.89 (m, 3H), 7.52 (dd, *J* = 11.2, 4.0 Hz, 1H), 7.41 (dd, *J* = 11.2, 4.0 Hz, 1H), 7.39 – 7.30 (m, 4H), 7.26 – 7.14 (m, 6H), 7.02 (d, *J* = 8.9 Hz, 2H); ^{13}C-NMR (CD_2Cl_2, 125 MHz, δ/ppm) 164.9, 154.5, 152.4, 147.2 (CH), 146.7 (CH), 135.4, 132.9 (2 x CH), 130.5 (4 x CH), 127.5 (CH), 127.1 (4 x CH), 126.3 (CH), 126.0 (2 x CH), 125.2, 123.8 (CH), 122.4 (CH), 120.2 (2 x CH), 118.0, 101.8 (CN); IR (ν/cm^{-1}) 3056, 2210 (ν_{CN}), 1570/1487/1506, 1430, 1174, 987; HRMS (ESI^+) calcd for $C_{28}H_{20}N_3S$ $[M+H]^+$: 430.1372, found: 430.1357; UV-Vis (CH_2Cl_2) λ_{max} = 454 nm (ε = 31 200 $L.mol^{-1}.cm^{-1}$).

2.2.11 (*E*)-2-[3-cyano-4-(4-(diphenylamino)styryl)-5,5-dimethylfuran-2(5*H*)-ylidene]malononitrile (1f). From **1** (546 mg, 2 mmol.) and *TCF* **F** (318 mg, 1.6 mmol.) following a slightly modified *general protocol 1*. Toluene (2 mL) was added in the initial mixture. The mixture was heated at 80°C for 24 h, then cooled to room temperature. The mixture was concentrated under *vacuum* and Et_2O (10 mL) was added to precipitate the compound. It was then filtered, washed with Et_2O (2x10 mL) and with ethanol (2x10 mL), and dried. **1f** was obtained as green solid (380 mg, yield = 53%); m.p. > 250°C (dec); ^{1}H NMR (500 MHz, $CDCl_3$, δ/ppm) 7.58 (d, *J* = 16.1 Hz, 1H), 7.46 (d, *J* = 8.4 Hz, 2H), 7.36 (t, *J* = 7.1 Hz, 4H), 7.20 (dd, *J* = 18.9, 7.4 Hz, 6H), 6.98 (d, *J* = 8.4 Hz, 2H), 6.82 (d, *J* = 16.1 Hz, 1H), 1.76 (s, 6H); ^{13}C NMR (125 MHz, $CDCl_3$, δ/ppm) 176.2, 174.3, 152.9, 147.6 (CH), 146.0, 131.5 (2 x CH), 130.2 (4 x CH), 126.7 (4 x CH), 126.3, 126.0 (2 x CH), 120.3 (2 x CH), 112.6, 111.8, 111.6 (CH), 111.3, 97.5 (2 x CN), 97.1 (CN), 56.6, 27.0 (2 x CH_3); IR (ν/cm^{-1}) 2223 (ν_{CN}), 1742, 1560, 1545, 1528, 1488, 1330, 1283, 1266, 1168, 758, 698; HRMS (ESI$^+$) calcd for $C_{30}H_{23}N_4O$ $[M+H]^+$: 455.1866, found: 455.1857; UV-Vis (CH_2Cl_2) λ_{max} = 565 nm (ε = 42 000 L.mol^{-1}.cm^{-1}).

2.2.12 3-cyano-4-[2-[4-(diphenylamino)phenyl]ethenyl]-5,5-dimethyl-2-butenolide (1g). From **1** (273 mg, 1 mmol) and **G** (151 mg, 1 mmol) in acetonitrile (2 mL) and toluene (0.5 mL) using *general protocol 2*. Purification by chromatography (EtOAc/Petroleum ether: 30/70) afforded the title compound **1g**. Red solid (340 mg, yield = 83%); m.p. 171°C; ^{1}H-NMR (CD_2Cl_2, 500 MHz, δ/ppm) 7.65 (d, *J* = 16.3 Hz, 1H), 7.49 (d, *J* = 8.8 Hz, 2H), 7.35 (t, *J* = 7.9 Hz, 4H), 7.17 (t, *J* = 7.8 Hz, 6H), 6.99 (d, *J* = 8.8 Hz, 2H), 6.75 (d, *J* = 16.3 Hz, 1H), 1.65 (s, 6H); ^{13}C-NMR (CD_2Cl_2, 125 MHz, δ/ppm) 177.1 (CO), 167.2, 151.9, 146.8, 146.0 (CH), 130.6 (2 x CH), 130.2 (4 x CH), 127.0, 126.6 (4 x CH), 125.5 (2 x CH), 120.8 (2 x CH), 113.3, 112.3 (CH), 96.7 (CN), 87.4, 26.4 (2 x CH_3); IR (ν/cm^{-1}) 2223 (ν_{CN}), 1735 (ν_{CO}), 1556, 1506, 1486, 1279, 1262, 1175, 697; HRMS (ESI$^+$) calcd for $C_{27}H_{22}N_2O_2Na$ $[M+Na]^+$: 429.7573, found: 429.1570; UV-Vis (CH_2Cl_2) λ_{max} = 484 nm (ε = 38 400 L.mol^{-1}.cm^{-1}).

2.2.13 3-methyl ester-4-[2-[4-(diphenylamino)phenyl]ethenyl]-5,5-dimethyl-2-butenolide (1h). From **1** (273 mg, 1 mmol.) and **H** (200 mg, 1 mmol.) following *general protocol 1* (80°C, 24 h).

Purification by chromatography (EtOAc/Pentane: 20/80) afforded the title compound **1h**. Yellow solid (350 mg, yield = 74%); m.p. 174 °C; ^{1}H-NMR ($CDCl_3$, 500 MHz, δ/ppm) 7.75 (d, *J* = 16.9 Hz, 1H), 7.46 (d, *J* = 8.7 Hz, 2H), 7.36 – 7.26 (m, 4H), 7.18 (d, *J* = 16.9 Hz, 1H), 7.15 – 7.11 (m, 6H), 7.01 (d, *J* = 8.7 Hz, 2H), 3.88 (s, 3H), 1.71 (s, 6H); ^{13}C-NMR ($CDCl_2$, 125 MHz, δ/ppm) 173.6, 167.7, 163.5, 151.0, 147.2, 143.3 (CH), 130.1 (4 x CH), 130.0, 128.5, 126.3 (4 x CH), 125.0 (2 x CH), 121.6 (2 x CH), 115.5 (CH), 114.9, 84.5, 52.5 (CH_3), 27.6 (2 x CH_3); IR (ν/cm^{-1}) 1736 (ν_{CO}), 1561, 1486, 1283, 1265, 1219, 1169, 1050, 760, 699; HRMS (ESI$^+$) calcd for $C_{28}H_{25}NO_4Na$ [M+Na]$^+$: 462.1676, found: 462.1656; UV-Vis (CH_2Cl_2) λ_{max} = 483 nm (ε = 31 300 L.mol^{-1}.cm^{-1}).

2.2.14 3-(2-benzothiazolyl)-4-[2-[4-(diphenylamino)phenyl]ethenyl]-5,5-dimethyl-2-butenolide (1i). From **1** (273 mg, 1 mmol.) and **I** (259 mg, 1 mmol.) in acetonitrile (3 mL) and toluene (0.5 mL) according to *general protocol 2*. The microwave irradiations were applied at 100°C for 3 h. Purification by chromatography (EtOAc/Cyclohexane: 30/70) afforded the title compound **1i**. Red solid (410 mg, yield = 80%); m.p. 165-170°C; ^{1}H-NMR (CD_2Cl_2, 500 MHz, δ/ppm) 8.83 (d, *J* = 17.0 Hz, 1H), 8.12 (d, *J* = 8.1 Hz, 1H), 7.99 (d, *J* = 7.8 Hz, 1H), 7.59 (d, *J* = 8.5 Hz, 2H), 7.51 (dd, *J* = 7.5 Hz, 1H), 7.43 (dd, *J* = 7.5 Hz, 1H), 7.35 – 7.27 (m, 5H), 7.20 – 7.10 (m, 6H), 7.07 (d, *J* = 8.1 Hz, 2H), 1.83 (s, 6H); ^{13}C-NMR (CD_2Cl_2, 125 MHz, δ/ppm) 170.7, 165.7, 159.2, 153.7, 150.7, 147.3, 142.5 (CH), 135.5, 130.1 (4 x CH), 130.0 (2 x CH), 129.3, 126.7 (CH), 126.2 (4 x CH), 125.9 (CH), 124.9 (2 x CH), 123.6 (CH), 122.1 (CH), 121.8 (2 x CH), 117.5 (CH), 116.2, 85.8, 27.8 (2 x CH_3); IR (ν/cm^{-1}) 1735, 1583, 1562, 1486, 1265, 1171, 1141, 1024, 975, 761, 753, 696; HRMS (ESI$^+$) calcd for $C_{33}H_{27}N_2O_2S$ [M+H]$^+$: 515.1788, found: 515.1776; UV-Vis (CH_2Cl_2) λ_{max} = 455 nm (ε = 34 900 L.mol^{-1}.cm^{-1}).

2.2.15 2-((9-ethyl-*9H*-carbazol-3-yl)methylene)-*1H*-indene-1,3(*2H*)-dione (2a). From **2** (340 mg, 1.5 mmol.) and **A** (175 mg, 1.2 mmol.), following *general protocol 1* (45°C, 26 h). Purification by chromatography (petroleum ether/EtOAc: 3/1 v/v) afforded the title compound **2a**. Orange solid (330 mg, yield = 78%); m.p. 230°C; ^{1}H-NMR (CD_2Cl_2, 500 MHz, δ/ppm) 9.46 (s, 1H), 8.72 (d, *J* = 8.7 Hz, 1H), 8.24 (d, *J* = 7.7 Hz, 1H), 8.08 (s, 1H), 8.01 (dd, *J* = 5.4, 2.7 Hz, 1H), 7.96 (dd, *J* = 5.2, 2.9 Hz, 1H),

7.88 – 7.75 (m, 2H), 7.60 – 7.49 (m, 3H), 7.35 (t, *J* = 7.4 Hz, 1H), 4.43 (q, *J* = 7.3 Hz, 2H), 1.48 (t, *J* = 7.3 Hz, 3H); ^{13}C-NMR (CD_2Cl_2, 125 MHz, δ/ppm) 191.4 (CO), 190.2 (CO), 148.8 (CH), 143.8, 143.0, 141.3, 140.5, 135.4 (CH), 135.2 (CH), 133.7 (CH), 129.0 (CH), 127.3 (CH), 126.3 (CH), 125.4 (CH), 124.1 (CH), 123.8 (CH), 123.3 (CH), 123.2 (CH), 121.4 (CH), 121.1 (CH), 110.0 (CH), 109.4 (CH), 38.6 (CH_2), 14.2 (CH_3); IR (ν/cm^{-1}) 3059, 1665 (ν_{CO}), 1571/1553/1471, 1129; HRMS (ESI$^+$) calcd for $C_{24}H_{18}NO_2$ $[M+H]^+$: 352.1332, found: 352.1328; UV-Vis (CH_2Cl_2) λ_{max} = 453 nm (ε = 44 800 L.mol^{-1}.cm^{-1}).

2.2.16 (*Z*)-3-(9-ethyl-9*H*-carbazol-3-yl)-2-(4-nitrophenyl)acrylonitrile (2b). From **2** (450 mg, 2 mmol.) and **B** (400 mg, 2.5 mmol.) following *general protocol 1* (45°C, 18 h). Purification by chromatography (CH_2Cl_2) afforded the title compound **2b**. Orange solid (240 mg, yield = 33%); m.p. 244°C; ^{1}H-NMR (DMSO-d_6, 300 MHz, δ/ppm) 8.82 (d, *J* = 1.4 Hz, 1H), 8.43 (s, 1H), 8.34 (d, *J* = 8.9 Hz, 2H), 8.25 (dd, *J* = 8.7, 1.7 Hz, 1H), 8.14 (d, *J* = 7.7 Hz, 1H), 8.04 (d, *J* = 8.9 Hz, 2H), 7.82 (d, *J* = 8.7 Hz, 1H), 7.70 (d, *J* = 8.2 Hz, 1H), 7.54 (t, *J* = 7.7 Hz, 1H), 7.31 (t, *J* = 7.5 Hz, 1H), 4.51 (q, *J* = 7.1 Hz, 2H), 1.35 (t, *J* = 7.1 Hz, 3H); ^{13}C-NMR (DMSO-d_6, 101 MHz, δ/ppm) 147.6 (CH), 146.8, 141.4, 141.1, 140.3, 127.2 (CH), 126.8 (CH), 126.4 (CH), 124.5 (2 x CH), 124.2, 123.6 (2 x CH), 122.5, 122.1, 120.4 (CH), 120.1 (CH), 118.5, 110.0 (CH), 103.8 (CN), 37.4 (CH_2), 13.8 (CH_3); IR (ν/cm^{-1}) 2208 (ν_{CN}), 1576/1515/1472, 1334, 1231, 1159; HRMS (ESI$^+$) calcd for $C_{23}H_{17}N_3O_2Na$ $[M+Na]^+$: 390.1213, found: 390.1207; UV-Vis (CH_2Cl_2) λ_{max} = 405 nm (ε = 21 300 L.mol^{-1}.cm^{-1}).

2.2.17 (*Z*)-3-(9-ethyl-9*H*-carbazol-3-yl)-2-(pyridine-4-yl)acrylonitrile (2c). From **2** (300 mg, 1.35 mmol.) and **C** (250 mg, 1.5 mmol.) following *general protocol 2* (60°C, 48 h). Purification by chromatography (petroleum ether, EtOAc: 6/1 v/v) afforded the title compound. Orange solid (130 mg, yield = 30%); m.p. 216°C; ^{1}H-NMR (DMSO-d_6, 300 MHz, δ/ppm) 8.84-8.64 (m, 3H), 8.45 (s, 1H), 8.24 (dd, *J* = 8.8, 1.6 Hz, 1H), 8.14 (d, *J* = 7.7 Hz, 1H), 7.85 – 7.66 (m, 4H), 7.59 – 7.49 (m, 1H), 7.30 (t, *J* = 7.4 Hz, 1H), 4.49 (q, *J* = 7.1 Hz, 2H), 1.33 (t, *J* = 7.1 Hz, 3H), ^{13}C-NMR (DMSO-d_6, 75 MHz, δ/ppm) 150.4, 147.0, 141.8, 141.3, 140.2, 127.1, 126.7, 124.0, 123.5, 122.4, 122.0, 120.3, 120.001,

119.4, 118.0, 109.9, 109.8, 103.3, 37.3, 13.7; IR (ν/cm^{-1}) 2926, 2214 (ν_{CN}), 1628, 1573/1492, 1234; HRMS (ESI$^+$) calcd for $C_{22}H_{18}N_3$ $[M+H]^+$: 324.1495, found: 324.1483; UV-Vis (CH_2Cl_2) λ_{max} = 389 nm (ε = 25 000 L.mol^{-1}.cm^{-1}).

2.2.18 (*E*)-2-(benzo[*d*]thiazol-2-yl)-3-(9-ethyl-9*H*-carbazol-3-yl)acrylonitrile (2d). From **2** (400 mg, 1.8 mmol.) and **D** (375 mg, 2.5 mmol.) following *general protocol 2* (40°C, 18 h). Purification by chromatography (CH_2Cl_2) afforded the title compound **2d**. Orange solid (680 mg, yield = 57%). m.p. 230°C; ^{1}H-NMR (CD_2Cl_2, 500 MHz, δ/ppm) 8.80 (s, 1H), 8.37 (s, 1H), 8.28 (dd, *J* = 8.7, 1.5 Hz, 1H), 8.19 (d, *J* = 7.8 Hz, 1H), 8.06 (d, *J* = 8.1 Hz, 1H), 7.95 (d, *J* = 8.0 Hz, 1H), 7.62 – 7.48 (m, 4H), 7.44 (t, *J* = 7.6 Hz, 1H), 7.34 (t, *J* = 7.0 Hz, 1H), 4.44 (q, *J* = 7.3 Hz, 2H), 1.48 (t, *J* = 7.3 Hz, 3H); ^{13}C NMR (125 MHz, CH_2Cl_2, δ/ppm) 164.8, 154.3, 148.8 (CH), 142.7, 141.2, 135.2, 128.7 (CH), 127.2 (2 x CH), 126.1 (CH), 124.7 (CH), 124.0, 123.6 (CH), 123.3, 122.1 (CH), 121.3 (CH), 120.8 (CH), 118.0, 109.8 (2 x CH), 101.8, 38.5 (CH_2), 14.2 (CH_3); IR (ν/cm^{-1}) 2361, 1576/1559/1469, 1233, 1128; HRMS (ESI$^+$) calcd for $C_{24}H_{18}N_3S$ $[M+H]^+$: 380.1216, found: 380.1207; UV-Vis (CH_2Cl_2) λ_{max} = 417 nm (ε = 20 300 L.mol^{-1}.cm^{-1}).

2.2.19 (*E*)-2-(3-cyano-4-(2-(9-ethyl-9*H*-carbazol-3-yl)vinyl)-5,5'-dimethylfuran-2(5*H*)-ylidene)malononitrile (2f). From **2** (340 mg, 1.5 mmol.) and **F** (380 mg, 1.9 mmol.) following *general protocol 1* (45°C, 48 h). Purification by chromatography (CH_2Cl_2/pentane: 1/1 then 2/1 v/v) afforded the title compound **2f**. Red solid (180 mg, yield = 30%); m.p. 230°C; ^{1}H-NMR (DMSO-d_6, 400 MHz, δ/ppm) 8.79 (d, *J* = 1.3 Hz, 1H), 8.27 (d, *J* = 7.7 Hz, 1H), 8.18 (d, *J* = 16.2 Hz, 1H), 8.07 (dd, *J* = 8.8, 1.5 Hz, 1H), 7.76 (d, *J* = 8.7 Hz, 1H), 7.70 (d, *J* = 8.2 Hz, 1H), 7.60 – 7.48 (m, 1H), 7.31 (dd, *J* = 11.1, 3.8 Hz, 1H), 7.26 (d, *J* = 16.2 Hz, 1H), 4.50 (q, *J* = 7.1 Hz, 2H), 1.83 (s, 6H), 1.34 (t, *J* = 7.1 Hz, 3H); ^{13}C NMR (DMSO-d_6, 101 MHz, δ/ppm) 177.4, 175.8, 149.9 (CH), 142.4, 140.3, 127.9 (CH), 126.9 (CH), 125.6, 123.9 (CH), 123.1, 122.3, 121.0 (CH), 120.3 (CH), 113.1, 112.3, 111.9 (CH), 111.5, 110.2 (CH), 110.1 (CH), 99.0, 96.0, 53.0, 37.4 (CH_2), 25.4 (2 x CH_3), 13.9 (CH_3); IR (ν/cm^{-1}) 2219 (ν_{CN}), 1542/1508/1490, 1394, 1106; HRMS (ESI$^+$) calcd for $C_{26}H_{20}N_4ONa$ $[M+Na]^+$: 427.1529, found:

427.1515 (calcd.); UV-Vis (CH_2Cl_2) λ_{max} = 510 nm (ε = 24 000 L.mol^{-1}.cm^{-1}).

2.2.20 (*E*)-methyl-4-(2-(9-ethyl-9*H*-carbazol-3-yl)vinyl)-5,5'-dimethyl-2-oxo-2,5-dihydrofuran-3-carboxylate (2h). From **2** (470 mg, 2.1 mmol.) and **H** (330 mg, 1.8 mmol.) following *general protocol 1* (50°C, 48 h). Purification by chromatography (Petroleum ether, EtOAc: 6/1 v/v) afforded the title compound **2h**. Orange solid (450 mg, yield = 65%); m.p. 218°C; ^{1}H-NMR (CD_2Cl_2, 400 MHz, δ/ppm) 8.35 (s, 1H), 8.16 (d, *J* = 7.7 Hz, 1H), 7.97 (d, *J* = 16.9 Hz, 1H), 7.81 (d, *J* = 8.6 Hz, 1H), 7.59 – 7.40 (m, 4H), 7.30 (t, *J* = 7.3 Hz, 1H), 4.40 (q, *J* = 7.1 Hz, 2H), 3.94 (s, 3H), 1.79 (s, 6H), 1.45 (t, *J* = 7.2 Hz, 3H); ^{13}C-NMR (CD_2Cl_2, 101 MHz, δ/ppm) 174.1, 167.95, 163.8, 145.4 (CH), 142.3, 141.2, 127.2 (CH), 126.4 (CH), 124.1, 123.4, 122.3 (CH), 121.2 (CH), 120.5 (CH), 115.3 (CH), 114.3, 109.8 (CH), 84.7, 52.7 (CH), 38.6, 27.8 (2 x CH_3), 14.3 (CH_3); IR (ν/cm^{-1}) 2364, 1759, 1572/1542/1490, 1333, 1213, 1123; HRMS (ESI$^+$) calcd for $C_{24}H_{23}NO_4Na$ [M+Na]$^+$: 412.1519, found: 412.1511; UV-vis (CH_2Cl_2) λ_{max} = 413 nm (ε = 22 590 L.mol^{-1}.cm^{-1}).

2.2.21 (*E*)-3-(benzo[*d*]thiazol-2-yl)-4-(2-(9-ethyl-9*H*-carbazol-3-yl)vinyl)-5,5'-dimethylfuran-2(5*H*)-one (2i). From **2** (300 mg, 1.3 mmol.) and **I** (420 mg, 1.6 mmol.) following *general protocol 1* (70°C, 48 h). Purification by chromatography (Petroleum ether, EtOAc: 6/1 v/v) afforded the title compound **2i**. Orange solid (240 mg, yield = 78%); m.p. 223°C; ^{1}H NMR (500 MHz, CD_2Cl_2, δ/ppm) .89 (d, *J* = 16.9 Hz, 1H), 8.35 (d, *J* = 1.1 Hz, 1H), 8.14 (d, *J* = 8.1 Hz, 1H), 8.08 (d, *J* = 7.7 Hz, 1H), 8.02 – 7.85 (m, 1H), 7.81 (dd, *J* = 8.6, 1.5 Hz, 1H), 7.58 – 7.30 (m, 6H), 7.21 (dd, *J* = 10.9, 3.8 Hz, 1H), 4.31 (q, *J* = 7.3 Hz, 2H), 1.78 (s, 6H), 1.36 (t, *J* = 7.3 Hz, 3H); ^{13}C NMR (125 MHz, CD_2Cl_2, δ/ppm) 170.7, 165.9, 159.2, 153.6, 144.3, 141.9, 141.0, 135.5, 127.4, 126.9, 126.6, 126.3, 125.8, 125.8, 123.9, 123.5, 123.2, 122.1, 122.0, 121.8, 120.9, 120.2, 117.0, 115.9, 109.8, 109.6, 87.3, 85.7, 38.3, 27.7, 24.7, 14.0, 13.7; IR (ν/cm^{-1}) 2364, 1748, 1559/1471/1457, 1233, 1122; HRMS (ESI$^+$) calcd for $C_{29}H_{24}N_2O_2SNa$ [M+Na]$^+$: 487.1451, found 487.1436; UV-Vis (CH_2Cl_2) λ_{max} = 452 nm (ε = 22 600 L.mol^{-1}.cm^{-1}).

2.2.22 (*E*)-4-(2-(9-ethyl-9*H*-carbazol-3-yl)vinyl)-5,5'-dimethyl-3-(phenylsulfonyl)furan-

2(5*H*)-one (2j). From **2** (320 mg, 1.4 mmol.) and **J** (320 mg, 1.2 mmol.) following *general protocol 1* (50°C, 48 h). Purification by chromatography (petroleum ether, EtOAc: 6/1 v/v) afforded the title compound **2j**. Orange solid (165 mg, yield = 29%); m.p. 224°C; ^{1}H-NMR (CD_2Cl_2, 500 MHz, δ/ppm) 8.4 (s, 1H), 8.35 (d, *J*=16.8 Hz, 1H), 8.18 (d, *J*=7.6 Hz, 1H), 8.10 (d, *J*=7.6 Hz, 2H), 7.91 (d, *J*=8.5Hz, 1H), 7.67 (t, *J*=7.3 Hz, 1H), 7.60-7.52 (m, 6H), 7.32 (t, *J*=7.3 Hz, 1H), 4.43 (q, *J*=7.2 Hz, 2H), 1.77 (s, 6H), 1.48 (t, *J*=7.2 Hz, 3H); ^{13}C NMR (125 MHz, CD_2Cl_2, δ/ppm) 172.2, 165.6, 147.3, 142.6, 141.2, 141.0, 134.5, 129.6, 128.9, 127.2, 126.6, 124.2, 123.3, 123.0, 121.7, 121.2, 120.6, 113.2, 110.1, 109.8, 85.7, 38.6, 27.8, 14.2; IR (ν/cm^{-1}) 1748, 1583/1529/1472, 1330, 1234, 1148; HRMS (ESI^{+}) calcd for $C_{28}H_{25}NO_4SNa$ $[M+Na]^+$: 494.1397, found 494.1378; UV-Vis (CH_2Cl_2) λ_{max} = 439 nm (ε = 26 100 L.mol^{-1}.cm^{-1}).

2.2.23 (*Z*)-3-(4-(9*H*-carbazol-9-yl)phenyl)-2-(4-nitrophenyl)acrylonitrile (3b). From **3** (500 mg, 1.85 mmol.) and **B** (450 mg, 2.78 mmol.) following *general protocol 1* (40°C, 18 h). Purification by chromatography (Petroleum ether/EtOAc: 6/1 v/v) afforded the title compound **3b**. Orange solid (430 mg, yield = 56%); m.p. 223°C; ^{1}H-NMR (CD_2Cl_2, 500 MHz, δ/ppm) 8.34 (d, *J* = 8.0 Hz, 2H), 8.23 (d, *J* = 7.8 Hz, 2H), 8.17 (d, *J* = 7.7 Hz, 2H), 7.93 (d, *J* = 7.9 Hz, 2H), 7.85 – 7.76 (m, 3H), 7.55 (d, *J* = 8.2 Hz, 2H), 7.46 (t, *J* = 7.6 Hz, 2H), 7.33 (t, *J* = 7.4 Hz, 2H); ^{13}C-NMR (CD_2Cl_2, 125 MHz, δ/ppm) 144.8, 140.8, 131.9, 127.4, 126.8, 124.9, 124.3, 121.2, 121.0, 117.7, 110.4; IR (ν/cm^{-1}) 2219, 1588/1511/1448, 1220, 1170; HRMS (EI) calcd for $C_{27}H_{17}N_3O_2$ $[M]^{+\cdot}$: 416.1315, found: 415.1317; UV-Vis (CH_2Cl_2) λ_{max} = 404 nm (ε = 21 110 L.mol^{-1}.cm^{-1}).

2.2.24 (*E*)-2-(4-(4-(9*H*-carbazol-9-yl)styryl)-3-cyano-5,5'-dimethylfuran-2(5*H*)-ylidene)malononitrile (3f). From **3** (270 mg, 1 mmol.) and **F** (240 mg, 1,2 mmol.) following *general protocol 1* (50°C, 18 h). Purification by chromatography (Pentane/EtOAc: 70/30 v/v) afforded the title compound **3f**. Black solid (175 mg, yield = 39%); m.p. > 260°C; ^{1}H-NMR (DMSO-d_6, 500 MHz, δ/ppm) 8.28 (d, *J* = 7.8 Hz, 2H), 8.22 (d, *J* = 8.5 Hz, 2H), 8.07 (d, *J* = 16.5 Hz, 1H), 7.83 (d, *J* = 8.6 Hz, 2H), 7.49 (ddd, *J* = 13.3, 9.4, 4.7 Hz, 4H), 7.39 – 7.27 (m, 3H), 1.86 (s, 6H); ^{13}C-NMR (DMSO-d_6, 125

MHz, δ/ppm) 176.9, 174.9, 146.0 (CH), 139.9, 139.4 (CH), 133.0, 131.1 (CH), 126.6 (CH), 126.3 (CH), 123.0 (CH), 120.5, 115.7, 112.5, 111.7, 110.7, 109.7 (CH), 99.6 (CN), 99.3 (2 x CN), 54.4, 25.0 (CH_3); IR (ν/cm^{-1}) 2989, 2223, 2202, 1567, 1553, 1165, 745; HRMS (ESI^+) calcd for $C_{30}H_{20}N_4ONa$ $[M+Na]^+$: 475.1529, found: 475.1516; UV-Vis (CH_2Cl_2) λ_{max} = 481 nm (ε = 29 700 $L.mol^{-1}.cm^{-1}$).

2.2.25 (*E*)-4-(4-(9*H*-carbazol-9-yl)styryl)-5,5'-dimethyl-2-oxo-2,5 dihydrofuran-3-carbonitrile (3g). From **3** (270 mg, 1 mmol.) and **G** (150 mg, 1 mmol.) following *general protocol 1* (70°C, 4 h. Purification by chromatography (EtOAc/Pentane: 30/70) afforded the title compound **3g**. Yellow solid (290 mg, yield = 72%); m.p. 203°C; ^{1}H-NMR ($CDCl_3$, 500 MHz, δ/ppm) 8.16 (d, *J* = 7.7 Hz, 2H), 7.88 (d, *J* = 8.4 Hz, 2H), 7.83 (d, *J* = 16.5 Hz, 1H), 7.73 (d, *J* = 8.4 Hz, 2H), 7.54 – 7.41 (m, 4H), 7.33 (t, *J* = 7.4 Hz, 2H), 6.98 (d, *J* = 16.4 Hz, 1H), 1.74 (s, 6H); ^{13}C-NMR ($CDCl_3$, 125 MHz, δ/ppm) 176.0, 166.0, 144.5 (CH), 141.1, 140.3, 132.7, 130.2 (2 x CH), 127.4 (2 x CH), 126.4 (2 x CH), 124.0, 120.9 (2 x CH), 120.7 (2 x CH), 115.4 (CH), 112.2, 109.9 (2 x CH), 99.4, 87.0, 26.1 (2 x CH_3); IR (ν/cm^{-1}) 2233 (ν_{CN}), 1763, 1585, 1516, 1449, 1334, 1276, 1231, 1219, 1172, 1069, 750, 723; HRMS (ESI^+) calcd for $C_{27}H_{20}N_2O_2Na$ $[M+Na]^+$: 427.1417, found: 427.1413; UV-Vis (CH_2Cl_2) λ_{max} = 421 nm (ε = 21 070 $L.mol^{-1}.cm^{-1}$).

2.2.26 (*E*)-methyl-4-(4-(9*H*-carbazol-9-yl)styryl)-5,5'-dimethyl-2-oxo-2,5-dihydrofuran-3-carboxylate (3h). From **3** (270 mg, 1 mmol.) and **H** (200 mg, 1 mmol.) following *general protocol 1* (80°C, 12 h). Purification by chromatography (Cyclohexane/EtOAc: 80/20 v/v) afforded the title compound **3h**. Yellow solid (330 mg, yield = 78 %); m.p. 174°C; ^{1}H-NMR (CD_2Cl_2, 500 MHz, δ/ppm) 8.16 (d, *J* = 7.7 Hz, 2H), 7.96 (d, *J* = 17.0 Hz, 1H), 7.88 (d, *J* = 8.3 Hz, 2H), 7.70 (d, *J* = 8.3 Hz, 2H), 7.50 (d, *J* = 8.2 Hz, 2H), 7.45 (t, *J* = 7.5 Hz, 2H), 7.40 – 7.29 (m, 3H), 3.94 (s, 3H), 1.78 (s, 6H); ^{13}C-NMR (CD_2Cl_2, 125 MHz, δ/ppm) 158.2, 152.9, 148.7, 127.6 (CH), 126.5, 125.8, 120.1, 115.6 (2 x CH), 113.2 (2 x CH), 112.2 (2 x CH), 106.5 (2 x CH), 106.4 (2 x CH), 104.3 (CH), 102.9, 95.9 (2 x CH), 86.0, 70.3, 38.3 (CH_3), 12.9 (2 x CH_3); IR (ν/cm^{-1}) 1748 (ν_{CO}), 1587, 1515, 1450, 1230, 1215, 1049, 746, 723; HRMS (ESI^+) calcd for $C_{28}H_{23}NO_4Na$ $[M+Na]^+$: 460.1519, found: 460.1506; UV-Vis

(CH_2Cl_2) λ_{max} = 397 nm (ε = 23 200 $L.mol^{-1}.cm^{-1}$).

2.2.27 (*E*)-4-(4-(9*H*-carbazol-9-yl)styryl)-3-(benzo[*d*]thiazol-2-yl)-5, 5'- dimethylfuran-2(5*H*)-one (3i). From **3** (270 mg, 1 mmol.) and **I** (260 mg, 1 mmol.) following *general protocol 1* (80°C, 24 h). Purification by chromatography (Pentane/EtOAc: 90/10 v/v) afforded the title compound **3i**. Orange solid (445 mg, yield = 86%); m.p. 142°C; ^{1}H-NMR ($CDCl_3$, 500 MHz, δ/ppm) 8.20 (dd, *J* = 8.0 Hz, 1H), 8.17 (d, *J* = 8.2 Hz, 2H), 8.01 (d, *J* = 7.9 Hz, 1H), 7.94 (d, *J* = 8.3 Hz, 2H), 7.72 (d, *J* = 8.4 Hz, 2H), 7.62 – 7.38 (m, 7H), 7.33 (t, *J* = 7.4 Hz, 2H), 1.90 (s, 6H); ^{13}C-NMR ($CDCl_3$, 125 MHz, δ/ppm) 170.0, 164.0, 158.0, 153.0, 140.5 (CH), 140.3, 139.4, 135.2, 134.6, 129.5 (2 x CH), 127.2 (2 x CH), 126.3 (CH), 126.1 (2 x CH), 125.6 (CH), 123.7, 123.6 (CH), 123.2 (CH), 120.2 (2 x CH), 117.9, 109.7 (2 x CH), 99.9 (CH), 85.4, 27.3 (2 x CH_3); IR (ν/cm^{-1}) 1736, 1595, 1574, 1513, 1448, 1333, 1313, 1269, 1226, 1170, 1143, 1026, 748, 723; HRMS (ESI^+) calcd for $C_{33}H_{25}N_2O_2S$ $[M+H]^+$: 513.1631, found: 513.1631; UV-Vis (CH_2Cl_2) λ_{max} = 417 nm (ε = 20 630 $L.mol^{-1}.cm^{-1}$).

2.3 Crystallography

Single crystals suitable for X-ray diffraction were grown by slow diffusion of diisopropylether in concentrated chloroform solution. CCDC 1560148 (**1a**), 1560149 (**1b**), 1564219 (**1d**), 837775 (**1e**), 1578107 (**1g**), 1560145 (**1i**), 1560146 (**2b**), 1564223 (**2i**), 1560147 (**2j**) and 1560150 (**3f**) contains the supplementary crystallographic data for this paper. These data can be obtained free of charge from The Cambridge Crystallographic Data Centre via www.ccdc.cam.ac.uk/data_request/cif.

2.4 Spectroscopic measurements and solid-state fluorescence

Absorption spectra were recorded on a JASCO V670 spectrophotometer. Fluorescence spectra (excitation and emission) were measured using a Horiba-Jobin Yvon Fluorolog-3 spectrofluorimeter equipped with a Hamamatsu R928 photomultiplier tube. Spectra were reference corrected for both the excitation source light intensity variation (lamp and grating) and the emission spectral response (detector and grating). All solvents were of spectrophotometric grade. Coumarine 153 and Rubrene were purchased from Acros. Solid-state measurements were performed using a calibrated integrative

sphere collecting all the emission (2π steradians covered with spectralon®), model F-3018 from Horiba Jobin Yvon. Because the emission tails extend far in the red emission range, the spectrofluorimeter detector response was checked by recording the emission of known red emitting compounds (4-(dimethylamino)-nitrostilbene, tetraphenylporphyrin and rhodamine 6G) and calibrated in consequence.[60] Absolute quantum yields were measured as previously reported.[41]

2.5 Agregation-induced Emission Measurements

Stock solutions (1 mM) of the desired compound were prepared in acetone. For each water fraction (f_w), 100 µL of this solution were added in a 2 mL volumetric flask, followed by the required volume of acetone. Water was then added one-shot to reach 2 mL.

3. Results and Discussion

3.1 Syntheses

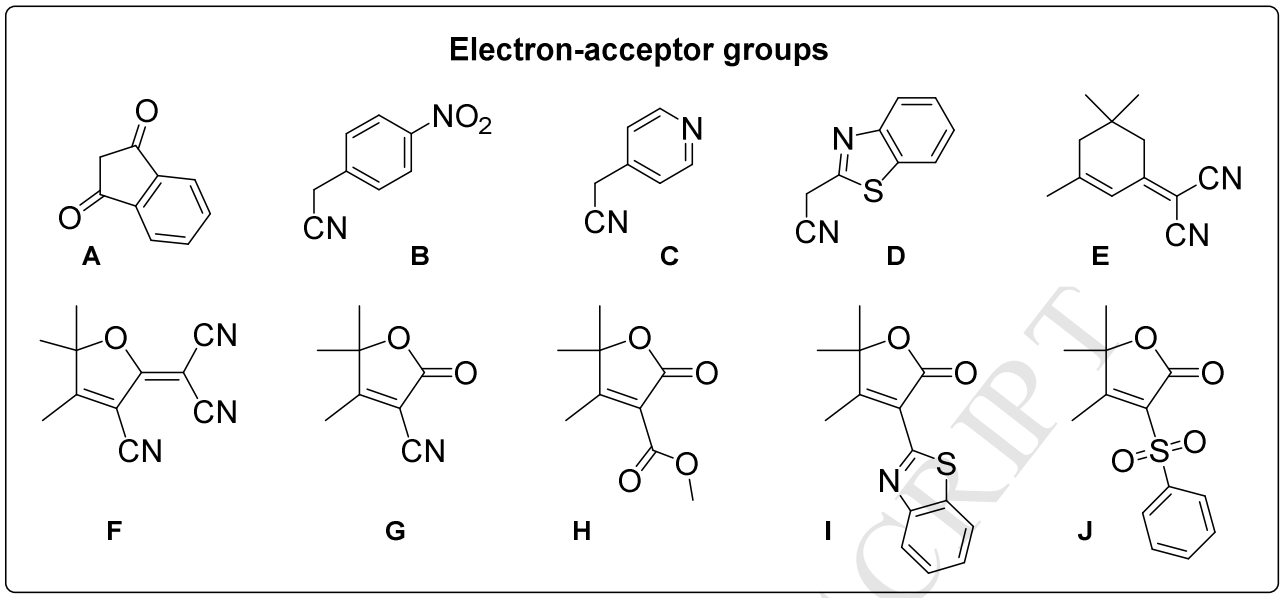

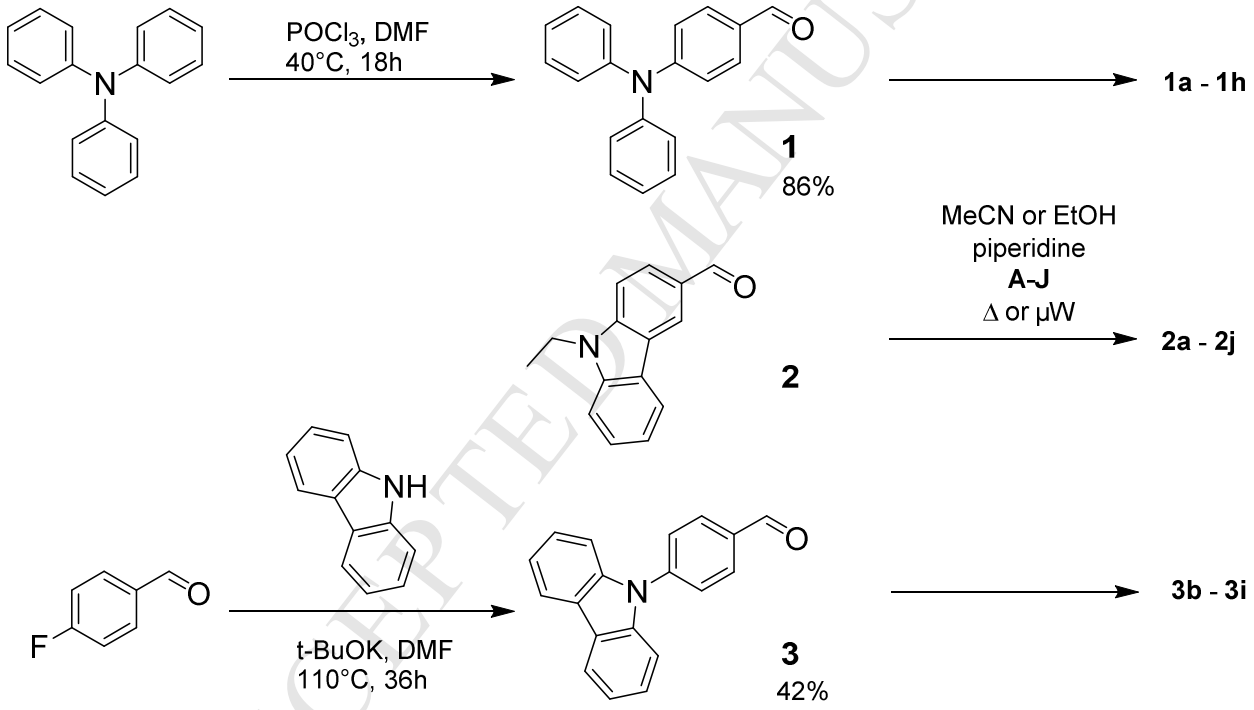

Scheme 1. Structures of activated methylene compounds **A**-**J** and synthesis of fluorophores **1a**-**1h**, **2a**-**2j** and **3b**-**3i**.

All compounds **1a – 3i** were prepared in moderate to good yield by a Knoevenagel condensation between 4-(diphenylamino)benzaldehyde **1**, 9-ethyl-9*H*-carbazole-3-carboxaldehyde **2** or 4-(9*H*-

carbazol-9-yl)-benzaldehyde **3** and the corresponding activated methylene compounds **A - J** in ethanol or acetonitrile in presence of catalytic amount of piperidine (Scheme 1). Conventional or microwave heating are used. Indanedione **A** and the 2-substitued acetonitrile derivatives **B - D** are commercially available. *Dicyanoisophorone* **E** was obtained from malonitrile and isophorone according to published procedure, whereas the 2(5*H*)-furanone ring *TCF* **F** was synthesized from malononitrile and 3-hydroxy-3-methyl-butan-2-one **4** with lithium ethoxide in ethanol as a base (Scheme 2).[61] Compounds **G - J** are 2-substituted-Δαβ-butenolide derivatives. The αβ-unsaturated-γ-lactone ring, also known as Δαβ-butenolide or 2(5*H*)-furanone, is a structural motif largely found in natural products such as vitamin C, cardenolide alkaloids or annonaceous acetogenin, to cite a few.[62-66] Therefore, substituted 2(5*H*)-furanone rings are interesting building blocks in organic chemistry and their syntheses have been largely investigated.[67-72] 4,5,5-trimethyl-2(5*H*)-furanone substituted at position C2 are obtained from 3-hydroxy-3-methyl-butan-2-one **4** as shown in Scheme 2. Thus, compounds **G** [68] and **H** [69] were obtained from **4** and ethyl cyanoacetate or dimethyl malonate, respectively, in presence of a catalytic amount of sodium methoxide in methanol. Subsequent reaction of **G** with 2-aminothiophenol in phosphoric acid afforded **I** in 66 % yield.[70] **J** was obtained in two steps from ethyl 2-bromoacetate by nucleophilic substitution with sodium sulfinate [53] followed by condensation with **4** in presence of sodium methoxide in methanol. The structures of all compounds **1a - 3j** were unambiguously assigned by ^{1}H and ^{13}C NMR. Although two isomers could potentially arise from the Knoevenagel condensation, the observation of one set of signals in the NMR spectra for the protons connected to the central C=C bond, consisting of one singlet or two doublets along with a ^{3}J coupling constant of 16 Hz, confirmed the stereoselective formation of the *Z*-isomers only for α-cyanostyrene derivatives (*i.e.* **1b-1d**, **2b-2d**, and **3b**) and of the *E*-isomer for the other styryl-derivatives (*i.e.* **1e-1i**, **2f-2j**, and **3f-3i**).

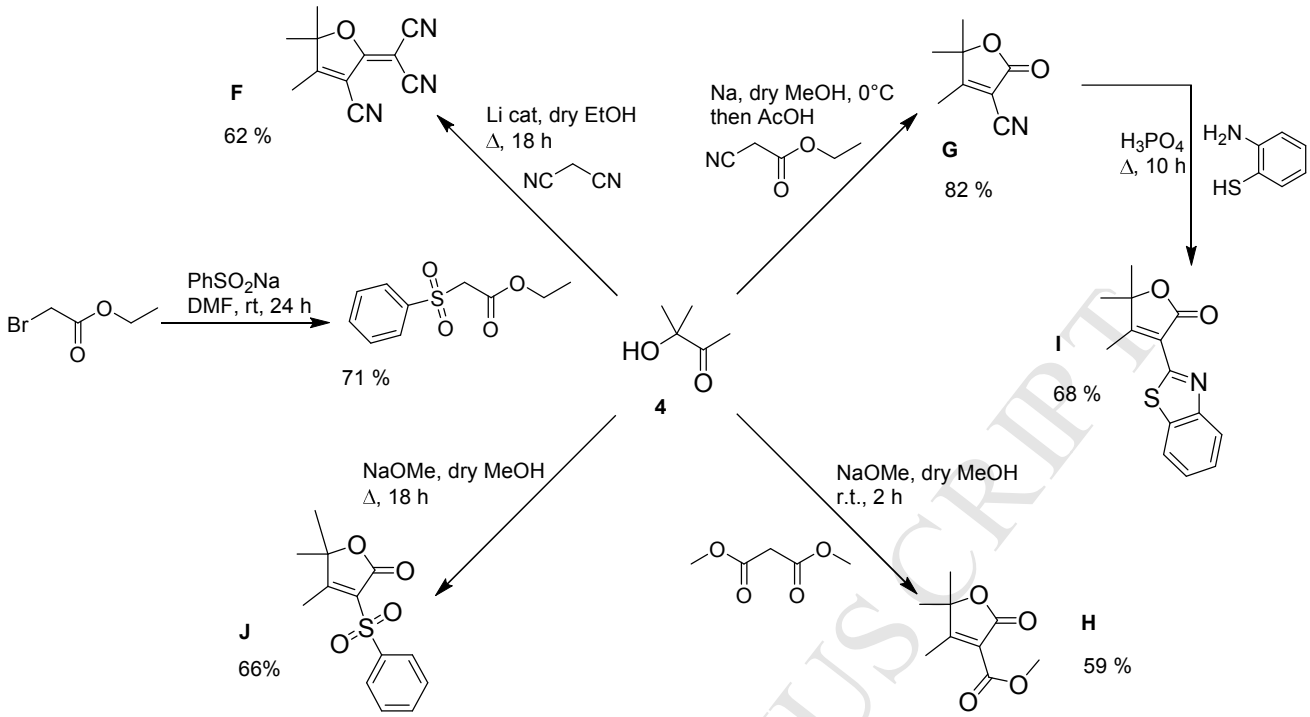

Scheme 2. Synthesis of the electron-accepting groups **F** - **J** from 3-hydroxy-3-methyl-butan-2-one **4**.

3.2 Photophysical Properties in Solution

The absorption spectra of all compounds were measured in diluted dichloromethane solutions. Relevant photophysical data are reported in Table 1. The spectra displayed in Figures 1 and SI-19 to SI-21 showed typical induced charge transfer transitions in the visible with bands positions varying accordingly with the strength of the substituent groups. For a given electron-donating group, increasing the electron-acceptor strength induced a red-shift of the absorption maxima: λ_{max} shifted from 427 nm for **1c** to 565 nm for **1f** bearing the strongest electron-withdrawing group in the 4-(*N*,*N*-diphenylamino)phenyl series, from 389 nm for **2c** to 510 nm for **2f** in the 9-ethyl-9*H*-carbazolyl series, and from 397 nm for **3h** to 481 nm for **3f** in the 4-(9*H*-carbazol-9-yl) series. In all cases, the strongest electro-accepting group **F** led to the most red-shifted absorption. Upon excitation in the main absorption band only a weak fluorescence was observed for most compounds likely because of radiationless decay from TICT excited states (Figures 1, SI-22 to SI-24). Only compounds **1a**, **1e**, **1g**, **1h**, **1i**, **3g**, and **3i**

displayed significant emission (Φ > 2%), up to 20% at 689 nm for **1e**. This low emission could be anticipated especially for molecules built on the α-cyano-stilbene motif (**1b**, **1c**, **1d**, **2b**, **2c**, **2d**, **3b**) that undergo very efficient non-radiative de-excitations via twisted conformations of chromophores in solution, torsional movements around the central C=C double bond [73-76] or cis-trans isomerization.[77] Emissions are characterized by large Stokes' shifts ranging from 1328 cm^{-1} for **2a** to 9462 cm^{-1} for **3b**, typical of an excited state charge transfer and of high difference between dipole moments in ground and excited states. Even though this is not the object of the present article, this latter parameter is important in view of obtaining large biphotonic fluorescence efficiencies, a plus for potential biological applications. On the other hand, the emission maxima ~~on the other hand~~ ranged from 502 nm (**2d**) to over 700 nm for the most red-shifted compounds **1b** (717 nm), **1f** (746 nm) and **3f** (712 nm). Given the importance of NIR emission for deep *in vivo* imaging,[78] such long emission wavelengths are interesting in spite of the low emission quantum yields, particularly for such small molecular weight molecules (molecular weight below 460 $g.mol^{-1}$).

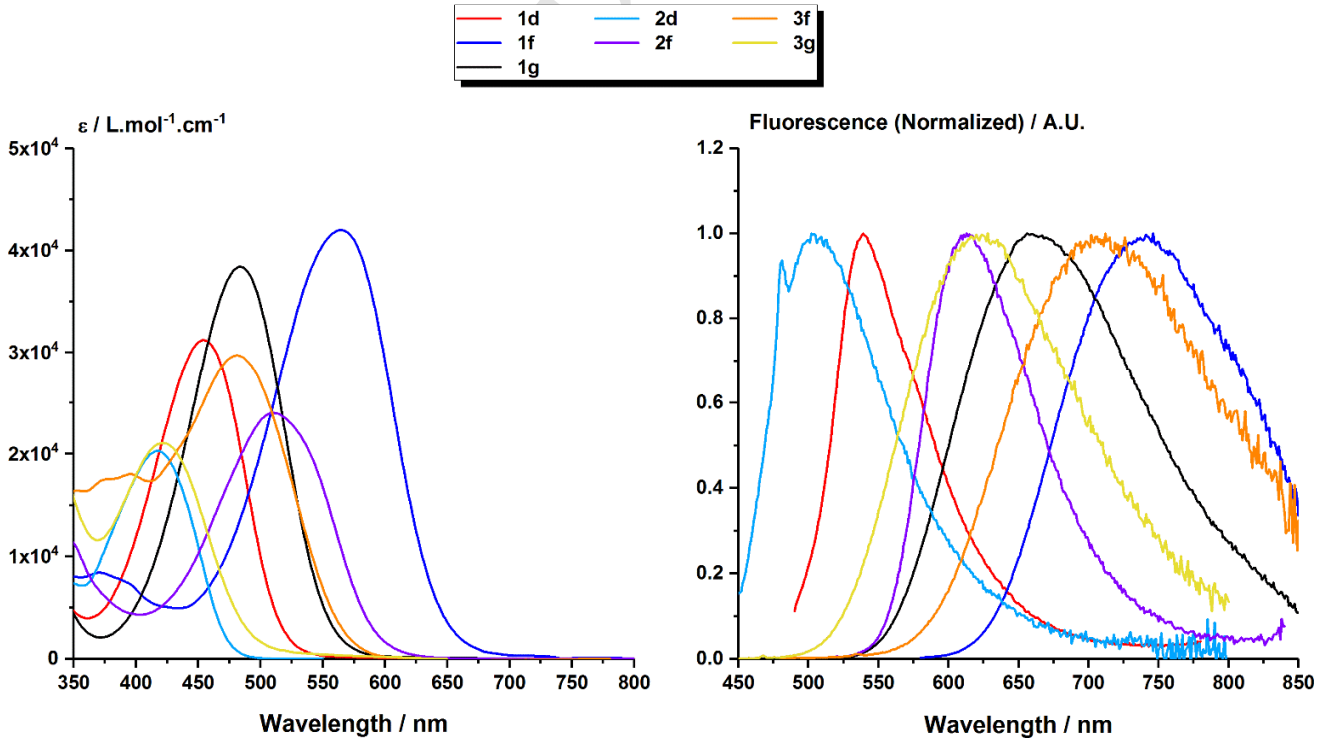

Figure 1. Absorption and emission spectra in dilute solution (CH_2Cl_2) for selected compounds.

Table 1. Spectroscopic data in dilute solution (CH_2Cl_2) and in the crystal state for all compounds.

Compound	Solution in CH_2Cl_2				Crystal state [c]	
	λ_{abs} / nm (ε / L.mol^{-1}.cm^{-1})	λ_{em} / nm	Φ [a] / %	$\Delta\nu$ / cm^{-1} [b]	λ_{em} / nm	Φ [d] / %
1a	485 (37800)	644	2	5091	618	11
1b	456 (28700)	717	<1	7983	669	4
1c	427 (29700)	572	<1	5937	640	23
1d	454 (31200)	539	<1	3474	647	18
1e	490 (23600)	689	20	5894	n.a.	n.a.
1f	565 (42000)	746	1	4294	n.a.	n.a.
1g	484 (38400)	656	6	5417	645	9
1h	455 (34900)	636	3	6255	640	10
1i	455 (34900)	633	7	5054	673	19
2a	453 (44800)	482	<1	1328	599	18
2b	405 (21300)	616	<1	8458	603	28
2c	389 (25000)	471	<1	4476	551	10
2d	417 (20300)	502	<1	4060	619	11
2f	510 (24000)	613	2	3295	768	4
2h	413 (22590)	576	<1	6852	583	8
2i	452 (22600)	533	<1	3362	614	34
2j	439 (26100)	546	<1	4464	598	33
3b	404 (21110)	654	<1	9462	596	11
3f	481 (29700)	712	<1	6745	735	11
3g	421 (21070)	628	6	7829	622	24
3h	397 (23200)	593	2	8326	534	24
3i	417 (20630)	583	4	6828	603	12

[a] Using Rubrene in methanol as reference (Φ = 27%) or Coumarine 153 in methanol (Φ = 54%). [b] Stokes' shifts. [c] In crystalline powder. [d] Using a calibrated integrated sphere.

3.2 Aggregation-Induced Emission

Aggregation-induced emission (AIE) fluorophores typically showed an increase in fluorescence intensity from the non-fluorescent or weakly fluorescent molecule in dilute organic solution to the strongly fluorescent suspension of nanoparticles that formed when water is added to the solvent. Good

AIE properties may be expected from solids that are strongly emissive in their crystalline state, although the emission wavelength and efficiency can be different, as we already noticed.[41]

The AIE behavior of some compounds was studied by recording the emission spectra obtained from acetone/water mixtures of fluorophores at the same concentration (10 µM), but with different volume fractions of water (f_w). The fluorescence of push-pull dipolar D-π-A compounds is usually weaker in polar solvents because enhanced electrostatic interactions with the chromophore strongly polarized ICT excited state. So as expected, the emission in pure acetone (f_w = 0) is significantly decreased in comparison with dichloromethane. The emission is further quenched when f_w was increased from 0 to 50-60% where the solvating power of the solvent mixture is still sufficient to dissolve the compounds and prevent aggregation, due to the higher polarity of the solvent system. Then, when f_w was gradually increased from 60% volume fractions of water to 95%, the products start to aggregate and form nanoparticles, whereas the fluorescence intensity increased considerably. Remarkably, all the compounds studied showed AIE, but noticeable differences could be evidenced as illustrated in Figure 2 and SI-25 to SI-35. On the other hand, the emission maxima of nanoparticles underwent a blue-shift with respect to pure acetone solution, for all compounds except **1d** (Fig. SI-28) and **2a** (Fig. SI-33). The maximum emission intensity was reached between 80 and 95% water volume fractions depending on the compound. In most cases, a decrease of the fluorescence intensity can be seen at higher f_w. The overall increase of fluorescence between solutions and nanoparticles (α_{AIE}) was of the order of α_{AIE} = *3-20* but could reach values higher than 100 for some compounds. Remarkable increases of more than *348* and *960* were obtained for **3g** and **3f** respectively, the most interesting compounds. This is reflected by the quantum yield values of nanoparticles, generally comprised between 2% and 8%, except for **3f** for which a noteworthy 20% quantum yield value at 678 nm was obtained, to be compared with the values measured in dichloromethane solution. It has to be noted that **1i** and **3g** are as fluorescent in their dissolved form in dichloromethane than in nanoparticles. Note that these results are in perfect agreement with those previously reported for compound **2a** (λ_{em} = 630 nm for a 15% quantum yield), although the

509 initial solvent used was not the same (THF instead of acetone here).[39]

510

511 **Table 2.** Optical properties in nanoparticles (acetone/water mixture).

Compound	Nanoparticles (acetone/water) [a]			
	λ_{abs} / nm	λ_{em} / nm	α_{AIE}	Φ / %
1a	493	635	106	8
1b	467	664	3	< 1
1c	437	595	20	2
1d	450	649	20	4
1e	490	698	9	3
1f	544	749	17	< 1
1g	489	659	136	6
1i	465	625	9	4
1h	493	636	59	5
2a	468 (460)[b]	630 (630)[b]	105	n.d (15%)[b]
3f	580	678	969	20
3g	425	616	348	8
3i	420	590	17	6

512 [a] In acetone/water at f_w giving the maximum emission. [b] according to [39]. THF solution was used
513 instead of acetone.

514

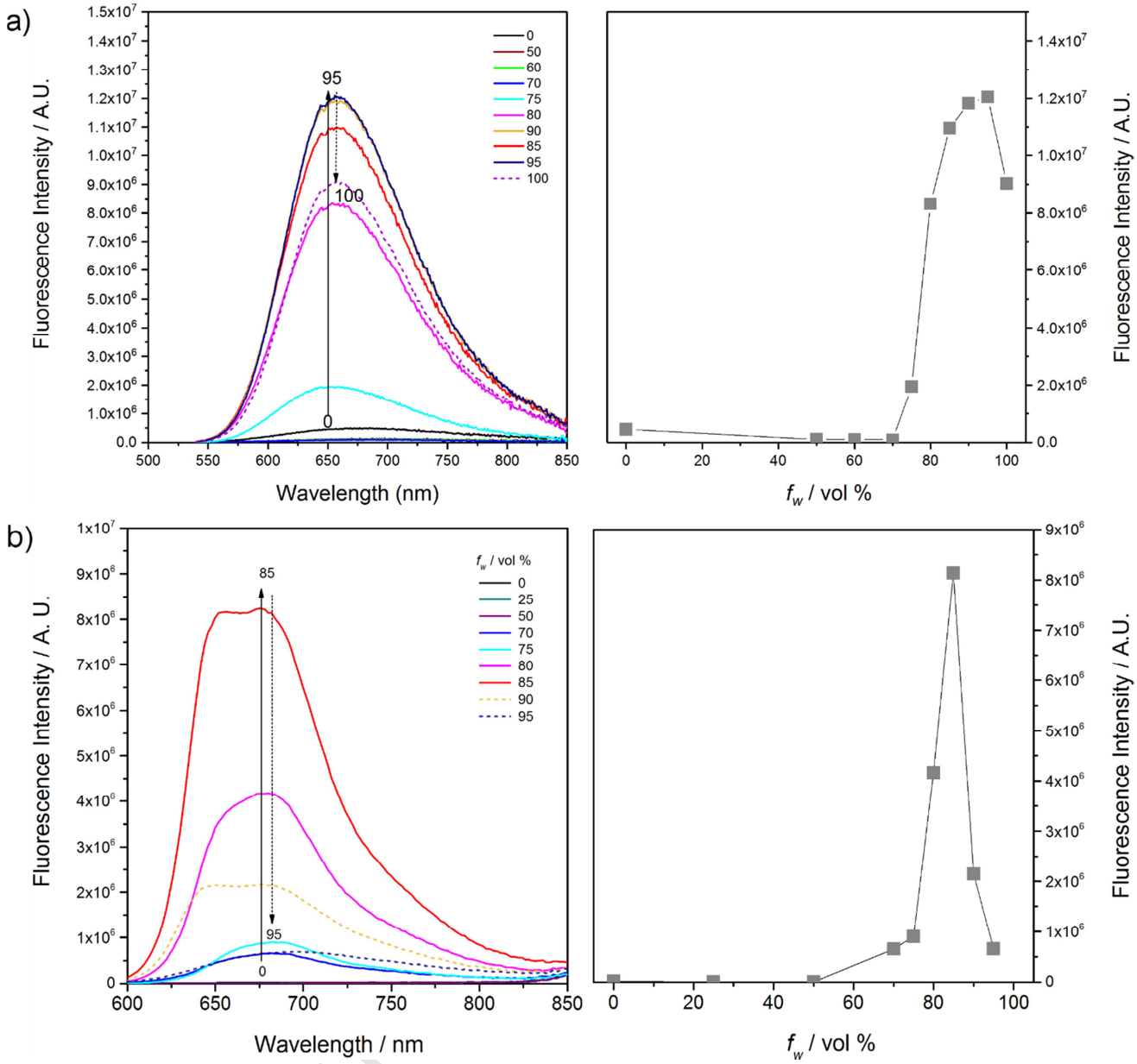

Figure 2. Emission spectra in acetone/water mixture of different water fraction (f_w), and change of the peak intensity with f_w for **1g** (a) and **3f** (b), c=10μM.

3.3 Emission in the Crystal State

Encouraged by the observations made in nanoparticles, we then turned our attention to the study of the emission in the crystal-state (micrometric powders). All compounds with the exception of **1e** and **1f** displayed an intense orange-red emission in their crystalline form under illumination by a handled UV lamp at 365 nm, visible to the naked eye. Emission and excitation spectra as well as fluorescence

quantum yields were therefore measured using a calibrated integrating sphere. Emission spectra are given in Figure 3 and in the Supporting Information (Figures SI-36 to SI-38) and data summarized in Table 1. In the crystal state, the emission was, in most cases, significantly red-shifted relative to the emission in solution in dichloromethane, 20 to 60 nm and up to 115 nm for compound **2d** displaying an emission maximum at 620 nm. Compounds **1a**, **1b**, **2b** and **3b**, for which a small blue shift (20 to 45 nm) was observed, were of notable exception. However, as expected, the strongest electron-accepting group (*TCF*) induces the maximum red-shift (compounds **2f** and **3f** having emission above 700 nm). The emission quantum yields were considerably increased though, reaching 34% at 614 nm for the most emissive compound **2i** and 11% at 735 nm for **3f**, which is remarkable for such small molecule.

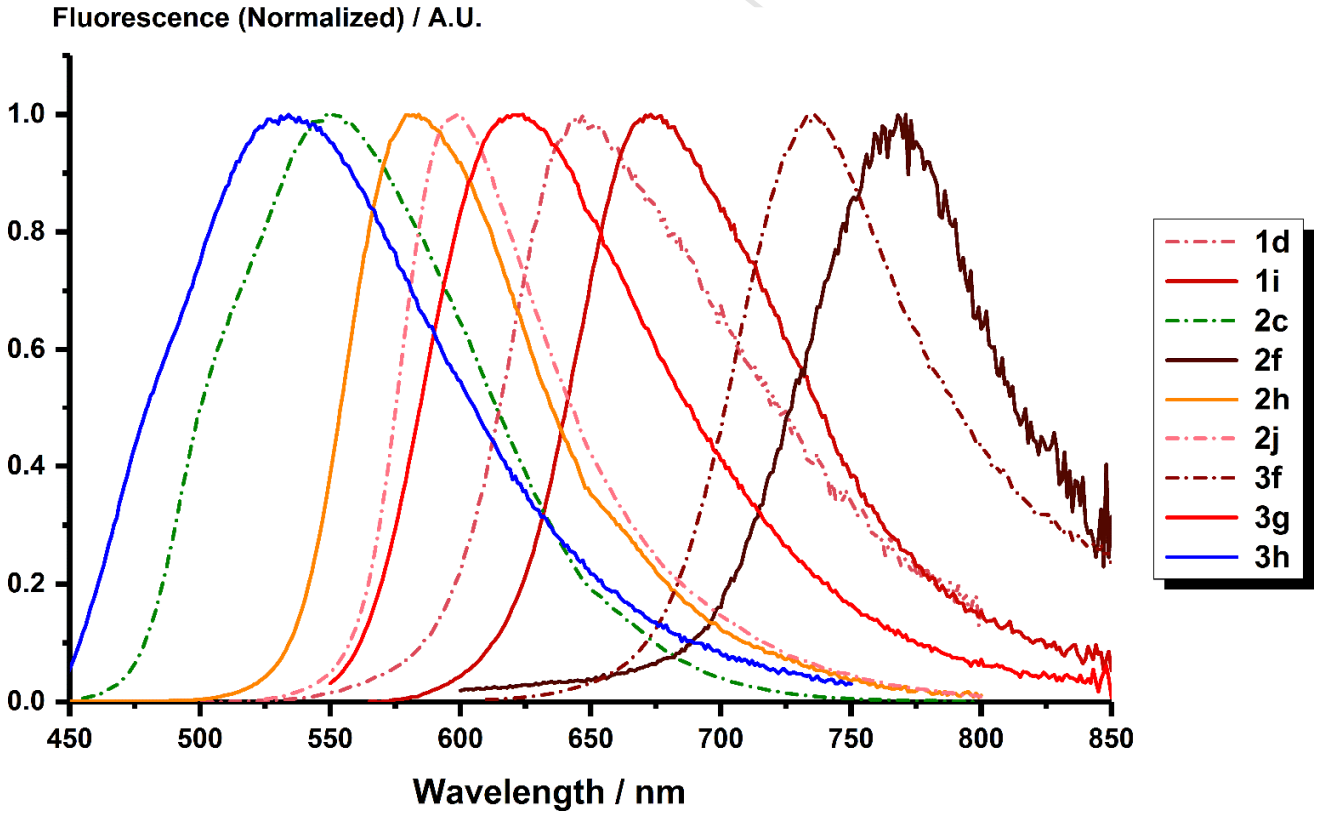

Figure 3. Crystal-state fluorescence spectra of selected compounds showing the tuning of emission wavelengths spanning the entire visible range.

3.4 Crystal structures

Although no study has directly linked the solid-state fluorescence properties to the crystalline structure, several have nevertheless pointed out that emission in solid may depend on the arrangements of the molecules in the crystal.[27, 79] Thus, on dipolar structure similar to those presented here, we have been able to show that certain patterns like ladder-like, brickwork or herringbone patterns could be observed in the crystal packing of emissive compounds, in which the molecules are slipped away with respect from one another preventing close packing.[40, 41] Conversely, the same studies associated the lack of crystal-state emission to the presence of closely packed face-to-face *H*-type dimers in the crystal structure. This was perfectly illustrated by the example of compounds **1e**, for which two molecules lie at short distance with respect to one another (3.587 Å) with strong π-π interactions (Figure 4).[40]

So knowledge of the crystal-state structure and the associated molecular packing could nevertheless help understanding the origin of the solid-state emission. To that end single crystals were grown by slow diffusion of a non-solvent (diisopropylether) in concentrated chloroform or dichloromethane solutions. Thus, we obtained sub-millimeter size crystal suitable for X-ray diffraction for nine new compounds over twenty-two synthesized and the structures were resolved (compounds **1a**, **1b**, **1d**, **1g**, **1i**, **2b**, **2j**, **2i** and **3f**). Crystallographic data and refinement parameters are given in Table 3, SI-2 and SI-3, whereas basic structural parameters, selected distances and dihedral angles are compiled in SI (Table SI-1) together with atom numbering schemes with the angles and distance definitions (Figure SI-1). ORTEP views with 50% probability are shown in Figures SI-2 to SI-10.

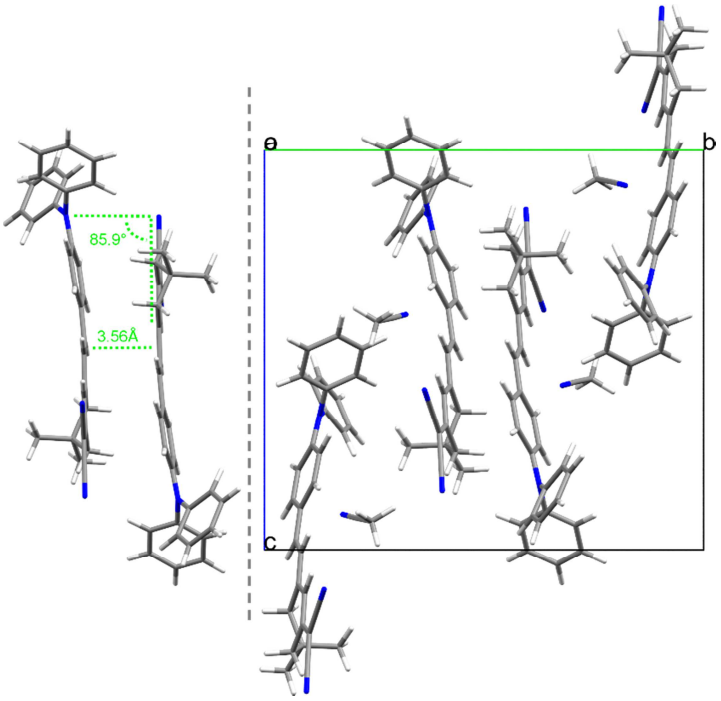

Figure 4. Compound **1e**, stacked dimer (left) and crystal packing view along the crystallographic *a* axis (right).

Compounds **1a** and **1d** crystallize in the $P\bar{1}$ triclinic space group. Compounds **1b**, **1e**, **1g**, **1i**, **2i** and **2j** crystallize in the $P2_1/n$ or $P2_1/c$ monoclinic space groups. **2b** and **3f** crystallize in the non-centrosymmetric orthorhombic $Fdd2$ and monoclinic $P2_1$ space groups respectively. The asymmetric units are composed of one molecule, except for **1d** and **1g** where two crystallographically independent molecules are present. As already observed for related dipolar molecules [40, 44, 80-82] or *N*,*N*-diethyl analogues,[40, 83] the molecular structures are very similar for all compounds with an almost planar π-conjugated system indicating a full conjugation between the donor and the acceptor end. Only the acceptor end of the dipole is slightly twisted with a dihedral angle measured between the main plane and the electron-accepting ring of 31.5° for the most distorted structures **1g** and **2j**, which is bend with a 14.4° angle between the 2(5*H*)-furanone ring mean plane and the carbazole ring mean plane. As expected the two phenyl groups on the *N*-donor atom are not coplanar with the main molecular plane for steric reasons but adopt a propeller type conformation.[25, 33] Such a conformation is not possible for

the carbazole ring in compound **3f** due to the additional C-C bond, but steric hindrance hampers the planarity and the carbazole ring is out of the main plane twisted by 35°. The carbazole rings of compounds **2b**, **2i** and **2j** on the other hand are fully planar and form the molecular plane as expected.[44] For compound **2j** finally, the phenyl ring of the phenyl sulfonyl group is almost perpendicular to the molecular plane (128°). Interestingly, for compound **1a** two aromatic C-C bonds of the donor para-phenylene ring, C*14*-C*15* [1.378 (3)] and C*30*-C*31* [1.379 (3) Å], are slightly shorter than the other four aromatic bonds [1.403 (4)-1.407 (3) Å] suggesting a para-quinoid character of the donor ring. Finally, whereas *s-trans* of the electron accepting group relative to the central double bond (b_1) was observed for most compounds, the two crystallographically independent molecules present in the unit cell of **1g** adopt different conformations, one being *s-trans* the other one *s-cis* (molecule A) and more twisted.

Here again, representative *J*-aggregates[84] in the form of ladder-like/brickwork (**1a**, **1d**, **2i**, **3f**) patterns, herringbone (**1b**, **1g**, **1i**, **2b**,) pattern, or both (**2j**), can be seen in the crystal packing of the fluorescent solids. Ladder-like and brickwork patterns are created by long chains of dipole lying one next to the other (**1a**, **1d**, **2i**, **2j**) or following each other (**3f**), that are stacked on top of each other. Two neighboring chains defining a common plane may point in the same direction (**1a**, **2j**, **3f**) or in the opposite direction (**1d**, **2i**), but are always shifted with respect to one another. Herringbone patterns, on the other hand, are built by broken lines of molecules following each other. In all cases, molecules are slipped away (**1a**, **1b**, **1d**, **1g**, **2b**, **2j**, **3f**) and/or tilted (**2b**, **2i**, **2j**) with respect from one another preventing close packing. The different patterns observed are schematized in Figures SI-11 to SI-18.

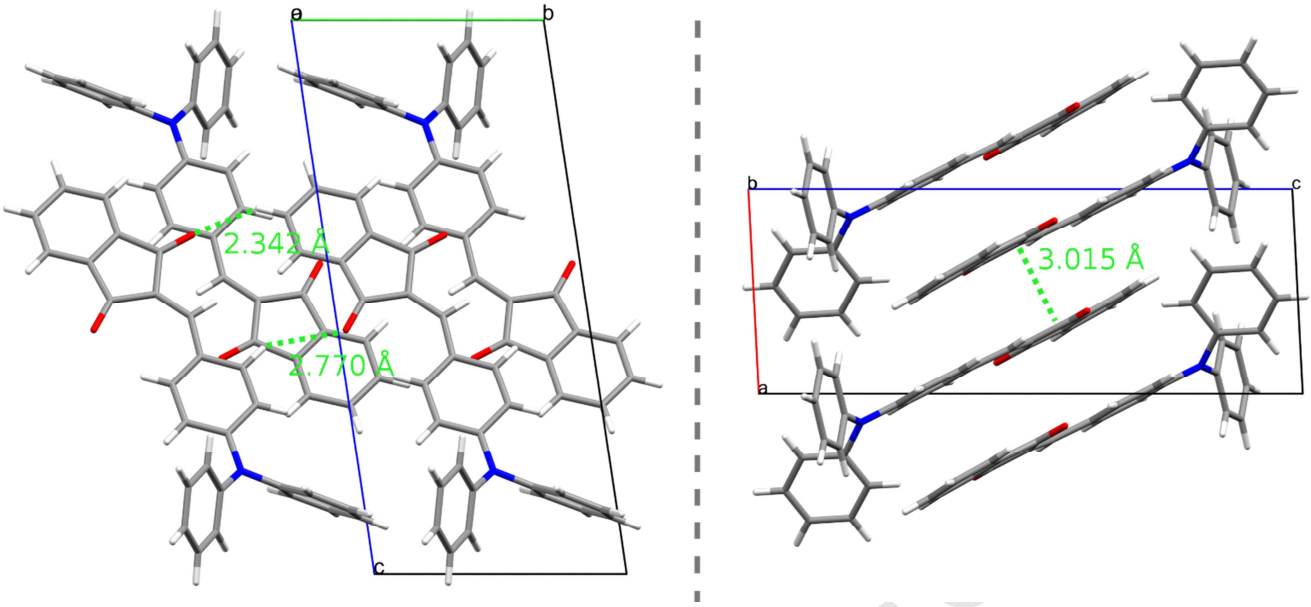

Figure 5. Crystal packing of **1a** view along the crystallographic *a* axis highlighting the brickwork pattern created by the H-bonds (left) and along the *b* axis showing the ladder-like pattern (right).

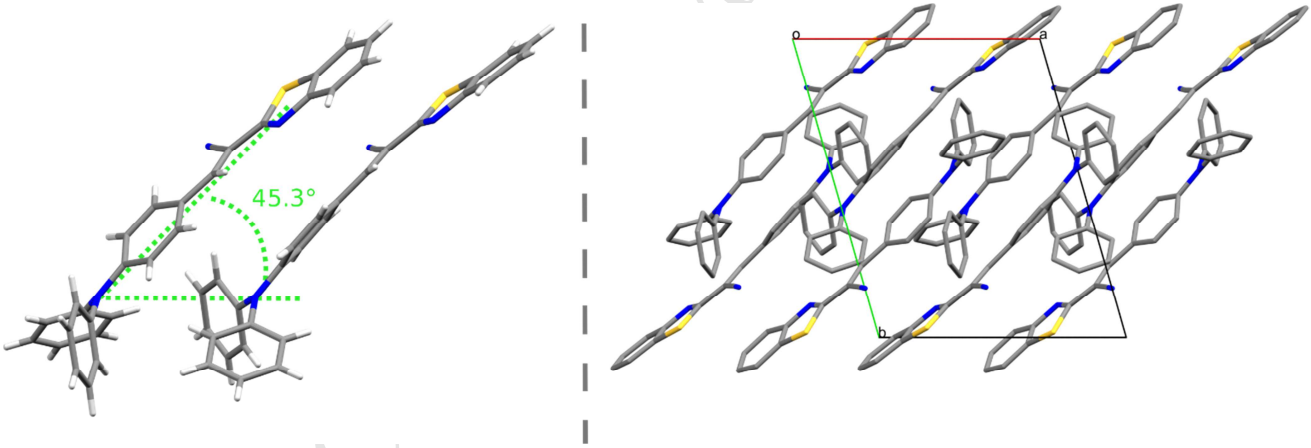

Figure 6. Crystal packing of **1d** showing the staircase arrangement of the two independent molecules (left) and repetition of the dimer motif along the c direction creating the ladder-like pattern (right), hydrogen atoms were removed for clarity.

So, the ladder-like crystal packing of **1a**, shown in Figure 5-right, is composed of juxtaposed dipoles all parallel to each other and interacting through long H-bonds (2.342 Å and 2.770 Å) between the C=O

groups and two aromatic C-H (Figure 5-left). This creates ribbons and a brickwork pattern growing in the *b* direction. Two neighboring bands, in which the dipoles are opposed and slightly slipped away longitudinally and transversally from each other, lies at a distance of 3.07 Å to each other. In the crystal packing of **1d**, the two independent molecules of the unit cells are oriented in the same direction, slipped away by 3.9 Å with a slip angle of almost 45°, archetype of staircase *J*-aggregate (Figure 6-left and Figure SI-11). Repetition of the dimeric motif along the *a* direction form a sheet parallel to the (*001*) plane in which all molecules are oriented in the same direction. Packing is formed by inversion of the sheet and translation along the *c* direction (Figure 6-right).

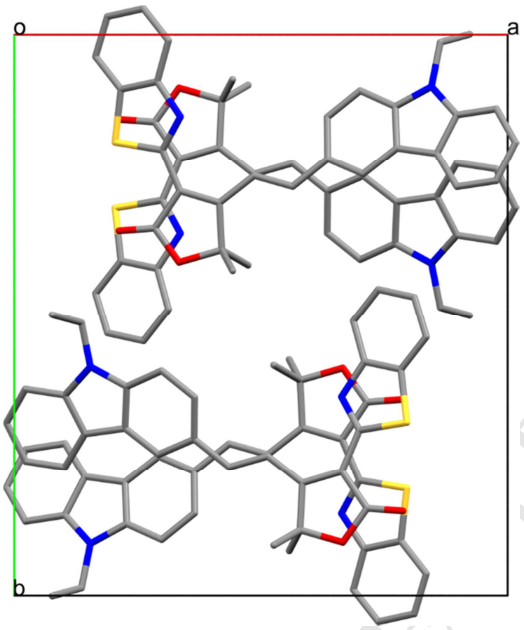

Figure 7. Crystal packing of **2i** viewed along the crystallographic *c* axis showing the classical brickwork pattern created by two juxtaposed head-to-tail slightly slipped away, hydrogen atoms were omitted for clarity.

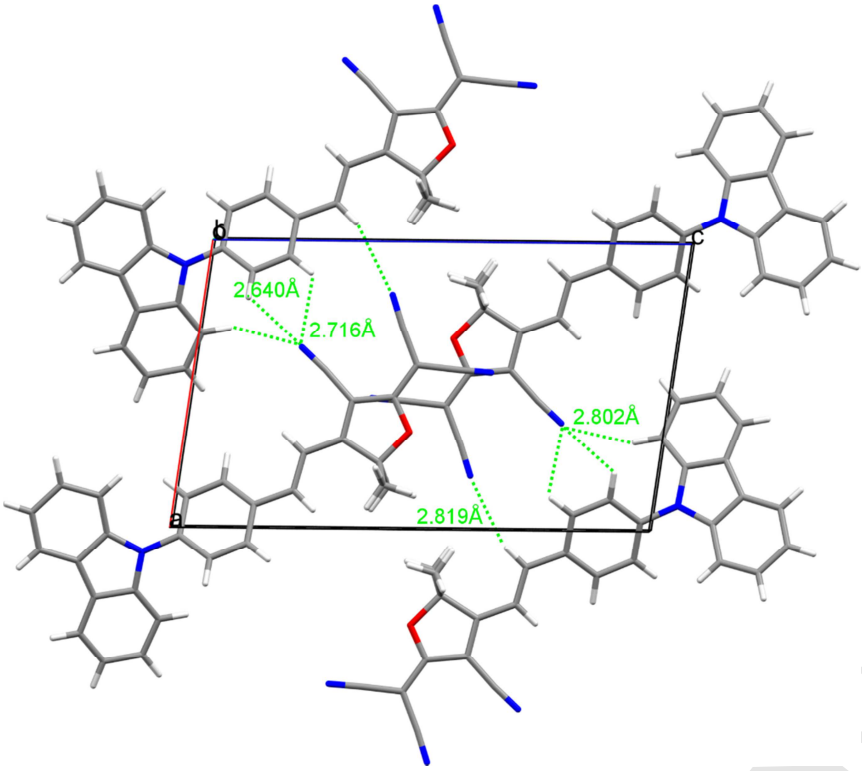

Figure 8. Crystal packing of **3f** viewed along the crystallographic *b* axis showing the brickwork pattern.

The crystal packing of **2i** (Figure 7) and **3f** (Figure 8) are best described in terms of infinite chains of in-line dipoles, slightly wavy in the case of **2i**. By translation along the axis perpendicular to the molecular one but in the molecular plane, parallel planes are formed creating the brickwork patterns, somewhat distorted in the case of **2i**. Two planes stand *ca* 3.5 Å (**3f**) and 3.7 Å (**2i**) apart (Figure SI-13 and SI-15). Within a plane, two neighboring chains are either parallel (**3f**) or anti parallel (**2i**) to each other. In the case of **3f**, two neighboring chains are connected through multiple weak H-bonds between C-H of the one molecule and the -C≡N group of the adjacent one. For **2i**, small inclination of two adjacent molecules with respect to each other draw waves propagating in the *a* and *c* directions. Note that among the compound emitting in the crystal state and nanoparticles, **3f** displayed the most red-shifted emission in solid and AIE.

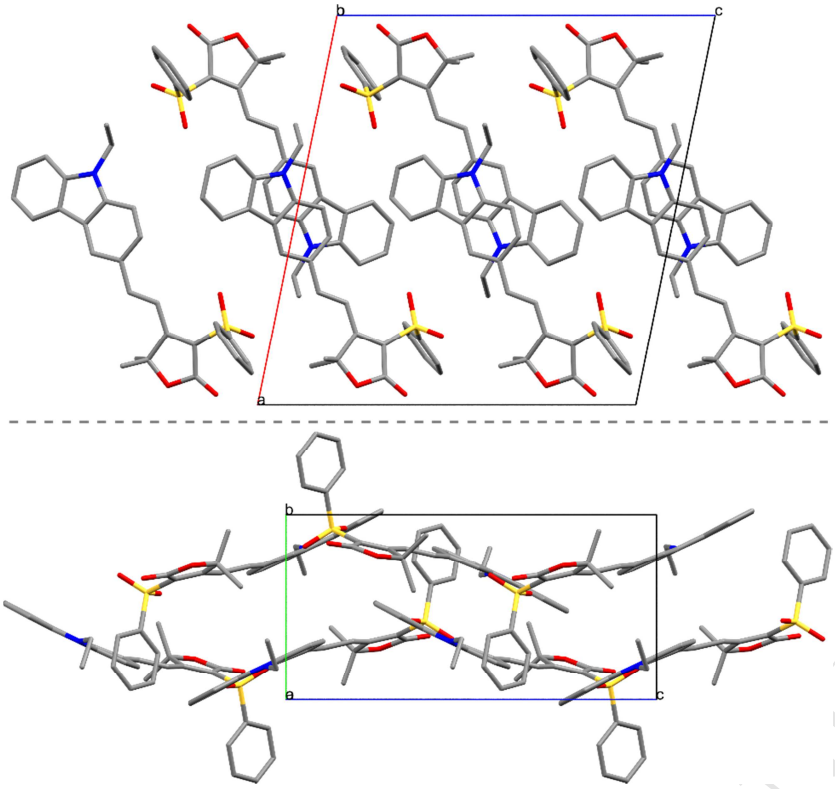

Figure 9. Crystal packing of **2j** viewed along *a* crystallographic showing the ladder-like pattern resulting from the repetition of head-to-tail molecules (top) and along *b* crystallographic axis showing the inclination of the molecules and the herringbone pattern (bottom). Note that Hydrogen atoms are omitted for clarity.

Compound **2j** crystal packing combines ladder-like and herringbone patterns. Stacks of head-to-tail molecules, 2.481 Å apart and considerably slipped away longitudinally by ca 5.8 Å, overlapping only at the level of the carbazole group, build the ladder growing along the *b* direction (Figure 9-top and Figure SI-14). On the other hand, two adjacent molecules, in which the benzenesulfonyl groups are placed alternatively above and below the mean plane of the molecular planes, are inclined with respect to each other forming an angle of 51°, creating an undulation along the *c* direction (Figure 9-bottom), sort of herringbone pattern. Note that **2j** (together with **2i**) present the highest emission quantum yield (respectively 33% and 34% at 598 nm and 614 nm respectively).

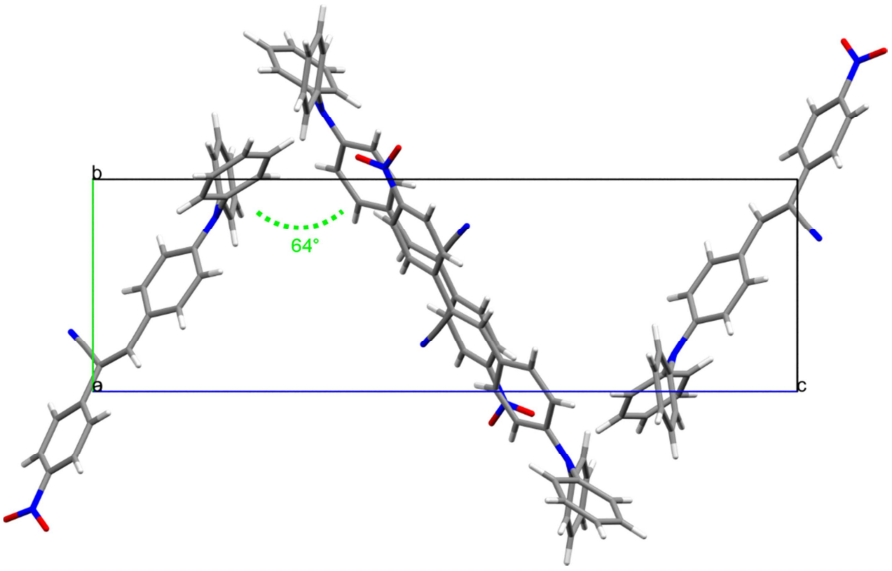

Figure 10. Crystal packing of **1b** viewed along *a* crystallographic axis showing the well-defined herringbone pattern.

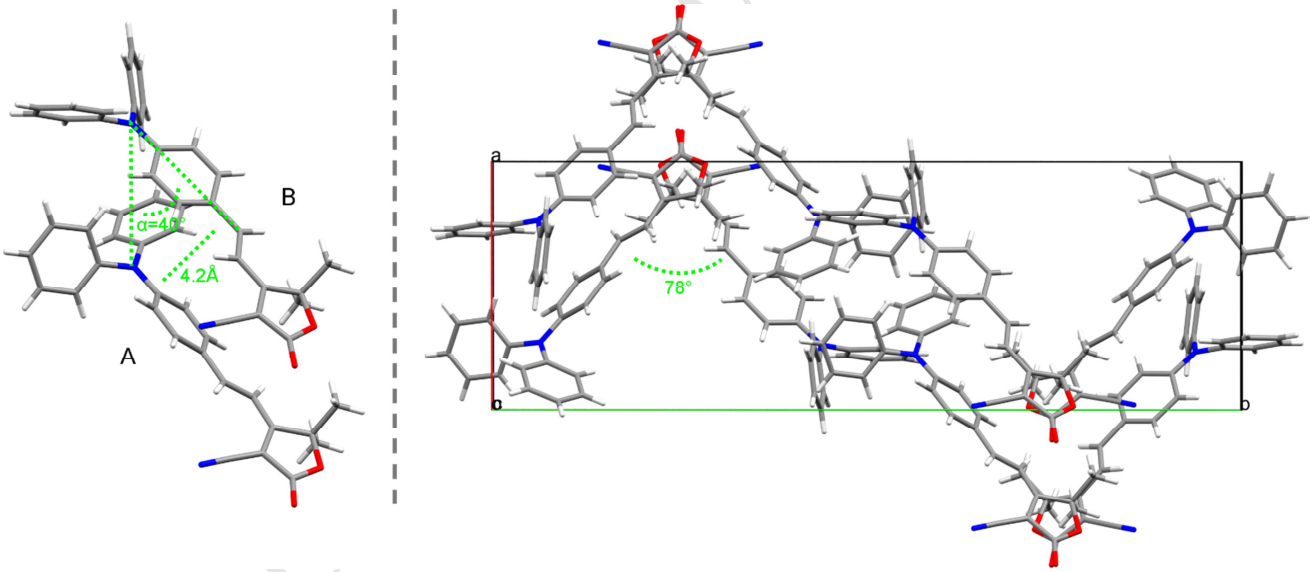

Figure 11. Crystal packing of **1g** viewed along *c* crystallographic axis showing the two independent molecules A and B (left) and the herringbone pattern (right). Notice the different the *s-cis* conformation of molecule A.

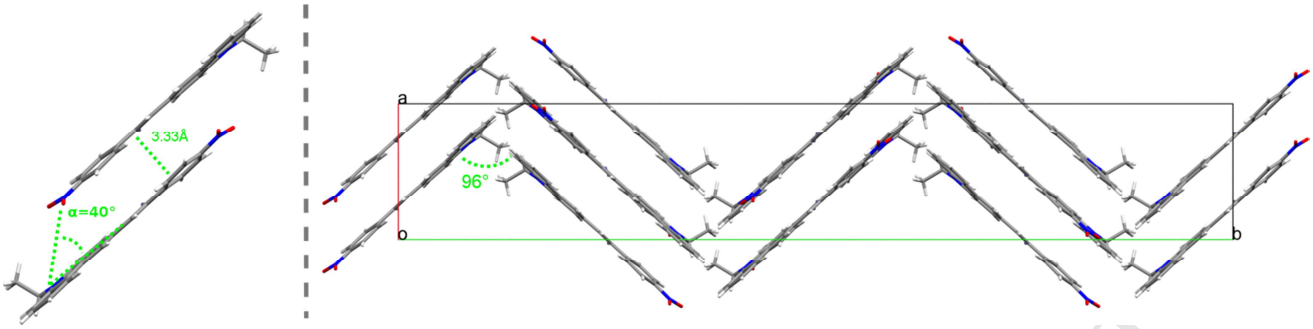

Figure 12. Crystal packing of **2b** viewed along *c* crystallographic axis showing the herringbone pattern (right) created by repetition of the dimer (left).

Well-ordered herringbone patterns are found in the packing of compounds **1b** (Figure 10), **1g** (Figure 11-right), and **2b** (Figure 12-right). For compound **1b** the four molecules of the unit cell arrange head-to-tail two-by-two forming accentuated vertices (64°). Two head-to-tail dipole are offset relative to one another slipped away both along the main molecular axis and perpendicular to that direction but in the molecular plane, preventing tight packing. **1b** is the compound displaying the weakest emission (4%). For compound **1g**, the two crystallographic independent molecules form a dimer (Figure 11-left). The two molecules are aligned in the same direction at roughly 4.2 Å apart but slipped away from 3.95 Å with a slip angle of 48°. Then four dimers arrange tail-to-tail then head-to-head in the unit cell forming a herringbone pattern growing in the *b* axis with vertices at 78° (Figure 11-right). The herringbone packing of **2b** is best viewed down crystallographic axis *c* (Figure 12-right). Obtuse vertices (96.5°) are formed by two broken lines of dimers. In the dimers the dipoles are anti-parallel to one another, lying 3.33 Å apart and are slipped away along the main molecular axis presenting a slip angle of ca 40° (Figure 12-left).

Finally, compound **1i** crystallized with one half disordered molecule of dichloromethane. The four molecules of the unit cell are almost in the same plane, rotated relative to each other by an angle of almost 90° about an axis passing through the centers (Figure 13) and connected by two 2 H-bonds (2.528 Å) between C=O and C-H benzothiazole ring of the closest nearby molecule. Dichloromethane

molecules are in the cell corner and intercalate in the center. Again, no close packing was observed in that structure explaining the good emission property obtained (19% at 673 nm).

So, characteristic aggregates are present in the crystalline structures of the emissive solids. To further identify the excitons responsible for solid emission, theoretical calculations are therefore now in progress based on the determined crystallographic structures.

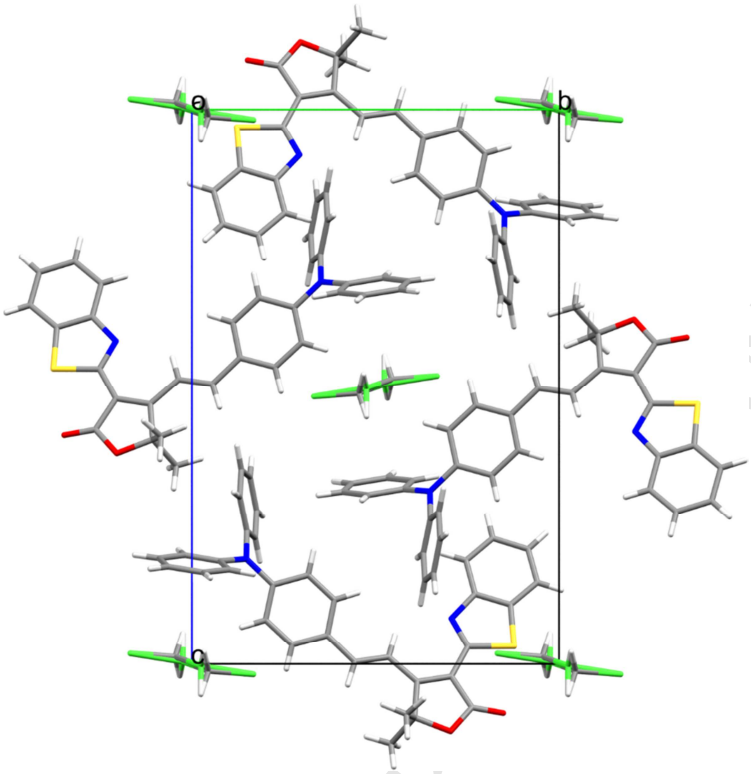

Figure 13. Crystal packing of **1i** viewed along *a* crystallographic axis.

680

681 **Table 3.** Crystal data parameters

	1a	**1b**	**1d**	**1e** [a]	**1g**	**1i**	**2b**	**2i**	**2j**	**3f**
Formula	$C_{28}H_{19}NO_2$	$C_{27}H_{19}N_3O_{22}$	2 ($C_{28}H_{19}N_3S$)	$C_{31}H_{27}N_3{\cdot}CH_3CN$	$C_{27}H_{22}N_2O_2$	$2(C_{33}H_{26}N_2O_2S){\cdot}CH_2Cl_2$	$C_{23}H_{17}N_3O_2$	$C_{29}H_{24}N_2O_2S$	$C_{28}H_{25}NO_4S$	$C_{30}H_{20}N_4O$
Cryst. Syst.	Triclinic	Monoclinic	Triclinic	Monoclinic	Monoclinic	Monoclinic	Orthorhombic	Monoclinic	Monoclinic	Monoclinic
Space group	$P\ \bar{1}$ (No. 2)	$P2_1/c$ (No. 14)	$P\ \bar{1}$ (No. 2)	$P2_1/c$ (No. 14)	$P2_1/n$ (No. 14)	$P2_1/n$ (No. 14)	$Fdd2$ (No. 43)	$P2_1/c$ (No. 14)	$P2_1/c$ (No. 14)	$P2_1$ (No. 4)
a (Å)	6.8190(10)	11.1416(9)	10.7820(10)	9.173 (5)	10.6973(4)	9.407(2)	9.1067(7)	16.006(3)	17.628(3)	10.0378(8)
b (Å)	8.1613(9)	7.5222(7)	14.020(4)	18.158 (5)	31.2560(10)	13.981(3)	55.697(5)	18.053(3)	8.2190(10)	7.0649(8)
c (Å)	18.129(2)	25.148(2)	16.248(2)	16.718 (5)	13.4698(6)	21.152(4)	14.2490(10)	8.2330(10)	16.809(2)	16.579(2)
α (°)	81.279(9)	90	73.790(10)	90.0	90	90	90	90	90	90
β (°)	86.530(10)	97.129(8)	81.800(10)	97.576 (5)	104.842(4)	92.61(2)	90	97.259(3)	101.55(2)	98.017(8)
γ (°)	86.000(10)	90	72.340(10)	90.0	90	90	90	90	90	90
V (Å^3)	993.5(2)	2091.3(3)	2242.8(7)	2760 (19)	4353.4(3)	2779.0(10)	7227.3(10)	2359.9(7)	2386.0(6)	1164.2(2)
Z	2	4	2	4	8	2	16	4	4	2

682 [a] Reference [40]

683

4. Conclusion

A library of twenty-two push-pull fluorophores featuring three different electron-donors groups, i.e. 4-(*N*,*N*-diphenylamino)phenyl-, 9-ethyl-9*H*-carbazolyl- or and 4-(9*H*-carbazol-9-yl)-, and various electron-acceptor groups were synthesized and their optical properties in solution, nanoparticle and crystal-state characterized. This study was supported by crystallographic analyses of the molecular packing in the crystal-state. Typical AIE was demonstrated by straightforward nanoprecipitation procedure involving solvent shifting process. The emission of the nanoparticles was characterized by red-shifted and enhanced emissions compared with the solution. For crystalline powders, intense emissions in the red and even in the far-red were achieved, reaching a remarkable 11% quantum yield for an emission at 735 nm. Confirming previous observations on push-pull dipolar solid-state emitters, the crystal-state emissions were related to the existence of specific molecular packing in the crystal structures. This study showed that considerable red-shift in the emission was possible by simple modulation of the strength of the electron-acceptor group, the same tendency being observed in nanoparticles and in the crystal-state although significant differences in the emission maxima wavelengths between the two states are noticed. Work has now started in exploiting the interesting crystal-state properties of the most emissive compounds for deep *in vivo* imaging. In particular, we aim at designing stable aqueous dispersions of bright crystalline fluorescent nanoparticles of defined size and narrow size distribution for which acquaintance with the physico-chemical parameters controlling the precipitation and the evolution of the suspension is required.

Acknowledgements

This work was funded by Région Rhône-Alpes through a PhD Grant for G E and financial support from Agence Nationale de la Recherche (ANR-11-BS08-0017 ULTRABRIGHT-TRACERS).

Supplementary data

Supplementary data related to this article include additional spectroscopic and crystallographic data

and figures, as well as complete ^{1}H and ^{13}C NMR data for all compounds.

References

[1] Peyghambarian N, Norwood RA. Organic optoelectronics: Materials and devices for photonic applications, part ii. Optics and Photonics News 2005;16(4):28-33.

[2] Wu H, Ying L, Yang W, Cao Y. Progress and perspective of polymer white light-emitting devices and materials. Chem Soc Rev 2009;38(12):3391-400.

[3] Reisch A, Klymchenko AS. Fluorescent polymer nanoparticles based on dyes: Seeking brighter tools for bioimaging. Small 2016;12(15):1968-92.

[4] Fery-Forgues S. Fluorescent organic nanocrystals and non-doped nanoparticles for biological applications. Nanoscale 2013;5(18):8428-42.

[5] Mei J, Leung NLC, Kwok RTK, Lam JWY, Tang BZ. Aggregation-induced emission: Together we shine, united we soar! Chem Rev 2015;115(21):11718-940.

[6] Qian J, Wang D, He S. Aggregation-induced emission dyes for in vivo functional bioimaging. Aggregation-induced emission: Fundamentals and applications, volumes 1 and 2: John Wiley and Sons Ltd; 2013. p. 209-37.

[7] Frangioni JV. In vivo near-infrared fluorescence imaging. Curr Opin Chem Biol 2003;7(5):626-34.

[8] Hilderbrand SA, Weissleder R. Near-infrared fluorescence: Application to in vivo molecular imaging. Curr Opin Chem Biol 2010;14(1):71-9.

[9] Ntziachristos V. Going deeper than microscopy: The optical imaging frontier in biology. Nat Meth 2010;7(8):603-14.

[10] Zhang X, Bloch S, Akers W, Achilefu S. Near-infrared molecular probes for *in vivo* imaging. Current Protocols in Cytometry 2012:Unit12.27.

730 [11] Mei J, Hong Y, Lam JWY, Qin A, Tang Y, Tang BZ. Aggregation-induced emission: The whole
731 is more brilliant than the parts. Adv Mater 2014;26(31):5429-79.

732 [12] Zhao Z, Geng J, Chang Z, Chen S, Deng C, Jiang T, *et al.* A tetraphenylethene-based red
733 luminophor for an efficient non-doped electroluminescence device and cellular imaging. J Mater Chem
734 2012;22(22):11018-21.

735 [13] Zhao Q, Li K, Chen S, Qin A, Ding D, Zhang S, *et al.* Aggregation-induced red-NIR emission
736 organic nanoparticles as effective and photostable fluorescent probes for bioimaging. J Mater Chem
737 2012;22(30):15128-35.

738 [14] Li K, Zhu Z, Cai P, Liu R, Tomczak N, Ding D, et al. Organic dots with aggregation-induced
739 emission (AIE dots) characteristics for dual-color cell tracing. Chem Mater 2013;25(21):4181-7.

740 [15] Ding D, Mao D, Li K, Wang X, Qin W, Liu R, *et al.* Precise and long-term tracking of adipose-
741 derived stem cells and their regenerative capacity via superb bright and stable organic nanodots. ACS
742 Nano 2014;8(12):12620-31.

743 [16] Jiang T, Qu Y, Li B, Gao Y, Hua J. Tetraphenylethene end-capped [1,2,5]thiadiazolo[3,4-
744 c]pyridine with aggregation-induced emission and large two-photon absorption cross-sections. RSC
745 Adv 2015;5(2):1500-6.

746 [17] Wang X, Morales AR, Urakami T, Zhang L, Bondar MV, Komatsu M, *et al.* Folate receptor-
747 targeted aggregation-enhanced near-ir emitting silica nanoprobe for one-photon in vivo and two-photon
748 ex vivo fluorescence bioimaging. Bioconjugate Chem 2011;22(7):1438-50.

749 [18] Wang Z, Yan L, Zhang L, Chen Y, Li H, Zhang J, *et al.* Ultra bright red AIE dots for cytoplasm
750 and nuclear imaging. Polym Chem 2014;5(24):7013-20.

751 [19] Zhao X, Xue P, Wang K, Chen P, Zhang P, Lu R. Aggregation-induced emission of
752 triphenylamine substituted cyanostyrene derivatives. New J Chem 2014;38(3):1045-51.

753 [20] Hang Y, Yang L, Qu Y, Hua J. A new diketopyrrolopyrrole-based near-infrared (nir) fluorescent
754 biosensor for BSA detection and AIE-assisted bioimaging. Tetrahedron Lett 2014;55(51):6998-7001.

755 [21] Gao Y, Feng G, Jiang T, Goh C, Ng L, Liu B, *et al.* Biocompatible nanoparticles based on diketo-
756 pyrrolo-pyrrole (DPP) with aggregation-induced red/NIR emission for *in vivo* two-photon fluorescence
757 imaging. Adv Funct Mater 2015;25(19):2857-66.

758 [22] Sanz N, Baldeck PL, Nicoud J-F, Le Fur Y, Ibanez A. Polymorphism and luminescence
759 properties of CMONS organic crystals: Bulk crystals and nanocrystals confined in gel-glasses. Solid
760 State Sci 2001;3(8):867-75.

761 [23] Treussart F, Botzung-Appert E, Ha-Duong N-T, Ibanez A, Roch J-F, Pansu R. Second harmonic
762 generation and fluorescence of cmons dye nanocrystals grown in a sol-gel thin film. ChemPhysChem
763 2003;4(7):757-60.

764 [24] Chen C-T. Evolution of red organic light-emitting diodes: Materials and devices. Chem Mater
765 2004;16(23):4389-400.

766 [25] Chiang CL, Wu MF, Dai DC, Wen YS, Wang JK, Chen CT. Red-emitting fluorenes as efficient
767 emitting hosts for non-doped, organic red-light-emitting diodes. Adv Funct Mater 2005;15(2):231-8.

768 [26] Ishow E, Brosseau A, Clavier G, Nakatani K, Tauc P, Fiorini-Debuisschert C, *et al.* Multicolor
769 emission of small molecule-based amorphous thin films and nanoparticles with a single excitation
770 wavelength. Chem Mater 2008;20(21):6597-9.

771 [27] Davis R, Saleesh Kumar NS, Abraham S, Suresh CH, Rath NP, Tamaoki N, *et al.* Molecular
772 packing and solid-state fluorescence of alkoxy-cyano substituted diphenylbutadienes: Structure of the
773 luminescent aggregates. J Phys Chem C 2008;112(6):2137-46.

774 [28] Ooyama Y, Uwada K, Kumaoka H, Yoshida K. Drastic solid-state fluorescence enhancement
775 behaviour of phenanthro[9,10-d]imidazole-type fluorescent hosts upon inclusion of carboxylic acids.

776 Eur J Org Chem 2009;2009(34):5979-90.

777 [29] D'Souza DM, Muschelknautz C, Rominger F, Müller TJJ. Unusual solid-state luminescent
778 push−pull indolones: A general one-pot three-component approach. Org Lett 2010;12(15):3364-7.

779 [30] Ooyama Y, Sugiyama T, Oda Y, Hagiwara Y, Yamaguchi N, Miyazaki E, *et al.* Synthesis of
780 carbazole-type d-π-a fluorescent dyes possessing solid-state red fluorescence properties. Eur J Org
781 Chem 2012;2012(25):4853-9.

782 [31] Gupta VD, Tathe AB, Padalkar VS, Umape PG, Sekar N. Red emitting solid state fluorescent
783 triphenylamine dyes: Synthesis, photo-physical property and dft study. Dyes Pigm 2013;97(3):429-39.

784 [32] Zheng Z, Yu Z, Yang M, Jin F, Zhang Q, Zhou H, *et al.* Substituent group variations directing
785 the molecular packing, electronic structure, and aggregation-induced emission property of isophorone
786 derivatives. J Org Chem 2013;78(7):3222-34.

787 [33] Yang M, Xu D, Xi W, Wang L, Zheng J, Huang J, *et al.* Aggregation-induced fluorescence
788 behavior of triphenylamine-based schiff bases: The combined effect of multiple forces. J Org Chem
789 2013;78(20):10344-59.

790 [34] Yang Q-Y, Lehn J-M. Bright white-light emission from a single organic compound in the solid
791 state. Angew Chem Int Ed 2014;53(18):4572-7.

792 [35] Wang L, Shen Y, Zhu Q, Xu W, Yang M, Zhou H, *et al.* Systematic study and imaging
793 application of aggregation-induced emission of ester-isophorone derivatives. J Phys Chem C
794 2014;118(16):8531-40.

795 [36] Ruanwas P, Boonnak N, Chantrapromma S. Five different colours solid-state fluorescence of
796 azastilbenes: A new push–pull π-conjugated system. Bull Mater Sci 2015;38(3):791-5.

797 [37] Zhang Y, Pan J, Zhang C, Wang H, Zhang G, Kong L, *et al.* High quantum yield both in solution

798 and solid state based on cyclohexyl modified triphenylamine derivatives for picric acid detection. Dyes
799 Pigm 2015;123:257-66.

800 [38] Lanke SK, Sekar N. Aggregation induced emissive carbazole-based push pull nlophores:
801 Synthesis, photophysical properties and dft studies. Dyes Pigm 2016;124:82-92.

802 [39] Singh A, Lim C-K, Lee Y-D, Maeng J-h, Lee S, Koh J, *et al.* Tuning solid-state fluorescence to
803 the near-infrared: A combinatorial approach to discovering molecular nanoprobes for biomedical
804 imaging. ACS Appl Mater Interfaces 2013;5(18):8881-8.

805 [40] Massin J, Dayoub W, Mulatier J-C, Aronica C, Bretonnière Y, Andraud C. Near-infrared solid-
806 state emitters based on isophorone: Synthesis, crystal structure and spectroscopic properties. Chem
807 Mater 2011;23(3):862-73.

808 [41] Ipuy M, Liao Y-Y, Jeanneau E, Baldeck PL, Bretonniere Y, Andraud C. Solid state red
809 biphotonic excited emission from small dipolar fluorophores. J Mater Chem C 2016;4(4):766-79.

810 [42] Cheng Y, Li G, Liu Y, Shi Y, Gao G, Wu D, *et al.* Unparalleled ease of access to a library of
811 biheteroaryl fluorophores via oxidative cross-coupling reactions: Discovery of photostable nir probe for
812 mitochondria. J Am Chem Soc 2016;138(14):4730-8.

813 [43] Shao A, Xie Y, Zhu S, Guo Z, Zhu S, Guo J, *et al.* Far-red and near-IR AIE-active fluorescent
814 organic nanoprobes with enhanced tumor-targeting efficacy: Shape-specific effects. Angew Chem Int
815 Ed 2015;54(25):7275-80.

816 [44] Ju H, Wan Y, Yu W, Liu A, Liu Y, Ren Y, et al. Structure and properties of a novel yellow
817 emitting material for organic light-emitting diodes. Thin Solid Films 2006;515(4):2403-9.

818 [45] Hou J, Pan Y, Jin J-Y, Wu X, Su Z-M. Isophorone-based analogues with A-π-D-π-A structure for
819 red organic light emitting devices. Synth Met 2009;159(5–6):401-5.

[46] Gao Z, Zhang X, Chen Y. Red fluorescence thin film based on a strong push–pull dicyanoisophorone system. Dyes Pigm 2015;113:257-62.

[47] Wang YJ, Shi Y, Wang Z, Zhu Z, Zhao X, Nie H, *et al.* A red to near-IR fluorogen: Aggregation-induced emission, large stokes shift, high solid efficiency and application in cell-imaging. Chem Eur J 2016;22(28):9784-91.

[48] Gao M, Su H, Li S, Lin Y, Ling X, Qin A, *et al.* An easily accessible aggregation-induced emission probe for lipid droplet-specific imaging and movement tracking. Chem Commun 2017;53(5):921-4.

[49] Zhang X, Gan X, Yao S, Zhu W, Yu J, Wu Z, *et al.* Branched triphenylamine-core compounds: Aggregation induced two-photon absorption. RSC Adv 2016;6(65):60022-8.

[50] Qi C, Ma H, Fan H, Yang Z, Cao H, Wei Q, *et al.* Study of red-emission piezochromic materials based on triphenylamine. ChemPlusChem 2016;81(7):637-45.

[51] Otomo A, Aoki I, Miki H, Tazawa H, Yokoyama S. Second-order nonlinear optical compounds with good nonlinear optical properties and heat resistance. National Institute of Information and Communications Technology, Japan; Sumitomo Electric Industries, Ltd.; Kyushu University, National University Corporation . 2011. p. 342pp.

[52] Moreno-Yruela C, Garin J, Orduna J, Franco S, Quintero E, Lopez Navarrete JT, *et al.* D-π-A compounds with tunable intramolecular charge transfer achieved by incorporation of butenolide nitriles as acceptor moieties. J Org Chem 2015;80(24):12115-28.

[53] Park CP, Nagle A, Yoon CH, Chen C, Jung KW. Formal aromatic C−H insertion for stereoselective isoquinolinone synthesis and studies on mechanistic insights into the C−C bond formation. J Org Chem 2009;74(16):6231-6.

[54] Monçalves M, Rampon DdS, Schneider PH, Rodembusch FS, Silveira CdC. Divinyl

843 sulfides/sulfones-based D–π–A–π–D dyes as efficient non-aromatic bridges for π-conjugated
844 compounds. Dyes Pigm 2014;102:71-8.

845 [55] Hauck M, Stolte M, Schönhaber J, Kuball H-G, Müller TJJ. Synthesis, electronic, and electro-
846 optical properties of emissive solvatochromic phenothiazinyl merocyanine dyes. Chem Eur J
847 2011;17(36):9984-98.

848 [56] Pan Q, Fang C, Zhang Z, Qin Z, Li F, Gu Q, *et al.* Synthesis and characterization of nonlinear
849 optical chromophores containing α-cyan with thermal stability. Opt Mater 2003;22(1):45-9.

850 [57] Percino MJ, Chapela VM, Cerón M, Castro ME, Soriano-Moro G, Perez-Gutierrez E, *et al.*
851 Synthesis and characterization of conjugated pyridine-(N-diphenylamino) acrylonitrile derivatives:
852 Photophysical properties. J Mater Sci Res 2012;1(2):181-2.

853 [58] Pérez-Gutiérrez E, Percino MJ, Chapela VM, Cerón M, Maldonado JL, Ramos-Ortiz G.
854 Synthesis, characterization and photophysical properties of pyridine-carbazole acrylonitrile derivatives.
855 Materials 2011;4(3):562.

856 [59] Cho MJ, Seo J, Oh HS, Jee H, Kim WJ, Kim KH, *et al.* Tricyanofuran-based donor–acceptor type
857 chromophores for bulk heterojunction organic solar cells. Sol Energy Mater Sol Cells 2012;98:71-7.

858 [60] Lakowicz JR. Appendix i. Corrected emission spectra. In: Lakowicz JR, editor. Principles of
859 fluorescence spectroscopy. Boston, MA: Springer US; 2006. p. 873-82.

860 [61] Briers D, Picard I, Verbiest T, Persoons A, Samyn C. Nonlinear optical active poly(adamantyl
861 methacrylate-methyl vinyl urethane)s functionalised with phenyltetraene-bridged chromophore.
862 Polymer 2004;45(1):19-24.

863 [62] Collins I. Saturated and unsaturated lactones. J Chem Soc, Perkin Trans 1 1999(11):1377-96.

864 [63] Rao YS. Recent advances in the chemistry of unsaturated lactones. Chem Rev 1976;76(5):625-

865 94.

866 [64] Zeng L, Ye Q, Oberlies NH, Shi G, Gu Z-M, He K, *et al.* Recent advances in annonaceous
867 acetogenins. Nat Prod Rep 1996;13(4):275-306.

868 [65] Tanzila MU, Vladimir VV. Advances in the synthesis of natural butano- and butenolides. Russ
869 Chem Rev 2009;78(4):337.

870 [66] Bassetti M, D'Annibale A. Formation of five- and six-membered α,β-unsaturated lactones
871 through ring-closing metathesis of functionalized acrylates. Applications to synthesis of natural
872 products. Curr Org Chem 2013;17(22):2654-77.

873 [67] Avetisyan AA, Dangyan MT. The chemistry of δ αβ -butenolides. Russ Chem Rev
874 1977;46(7):643.

875 [68] Avetisyan AA, Mangasaryan TA, Melikyan GS, Dangyan MT, Matsoyan SG. Unsaturated
876 lactones. Ii. Synthesis of unsaturated γ-lactones by condensation of α-ketoalcohols with acetoacetic and
877 cyanoacetic esters. Zh Org Khim 1971;7(5):962-4.

878 [69] Avetisyan AA, Tatevosyan GE, Mangasaryan TA, Matsoyan SG, Dangyan MT. Unsaturated
879 lactones. I. Synthesis of substituted unsaturated γ-lactones by condensing tertiary α-keto alcohols with
880 malonic ester. Zh Org Khim 1970;6(5):962-4.

881 [70] Melikyan GS, Avetisyan AA, Halgas J. Benzothiazole compounds. XLIII. Synthesis of
882 benzazoles with heterocyclic substituents and their condensation reactions with aldehydes. Chem Pap
883 1992;46(2):109-12.

884 [71] Avetisyan KS, Galstyan LK. Synthesis of 2-(2,5-dihydrofuran-3-yl)-2-oxoethyl carboxylates.
885 Russ J Org Chem 2013;49(6):936-9.

886 [72] Hakobyan RM, Hayotsyan SS, Melikyan GS. Cyclocondensation of 3-acetylfuran-2(5h)-ones

887 with benzylidenemalononitrile. Synthesis of 3-(5-amino-4,6-dicyanobiphenyl-3-yl)furan-2(5h)-ones.
888 Russ J Org Chem 2015;51(12):1809-12.

889 [73] An B-K, Kwon S-K, Jung S-D, Park SY. Enhanced emission and its switching in fluorescent
890 organic nanoparticles. J Am Chem Soc 2002;124(48):14410-5.

891 [74] An B-K, Gierschner J, Park SY. Π-conjugated cyanostilbene derivatives: A unique self-assembly
892 motif for molecular nanostructures with enhanced emission and transport. Acc Chem Res
893 2012;45(4):544-54.

894 [75] Oelkrug D, Tompert A, Egelhaaf H-J, Hanack M, Steinhuber E, Hohloch M, *et al.* Towards
895 highly luminescent phenylene vinylene films. Synth Met 1996;83(3):231-7.

896 [76] Oelkrug D, Tompert A, Gierschner J, Egelhaaf H-J, Hanack M, Hohloch M, *et al.* Tuning of
897 fluorescence in films and nanoparticles of oligophenylenevinylenes. J Phys Chem B
898 1998;102(11):1902-7.

899 [77] Font-Sanchis E, Galian RE, Cespedes-Guirao FJ, Sastre-Santos A, Domingo LR, Fernandez-
900 Lazaro F, *et al.* Alkoxy-styryl dcdhf fluorophores. PCCP 2010;12(28):7768-71.

901 [78] Mettra B, Appaix F, Olesiak-Banska J, Le Bahers T, Leung A, Matczyszyn K, *et al.* A
902 fluorescent polymer probe with high selectivity toward vascular endothelial cells for and beyond
903 noninvasive two-photon intravital imaging of brain vasculature. ACS Appl Mater Interfaces
904 2016;8(27):17047-59.

905 [79] Li Y, Li F, Zhang H, Xie Z, Xie W, Xu H, *et al.* Tight intermolecular packing through
906 supramolecular interactions in crystals of cyano substituted oligo(para-phenylene vinylene): A key
907 factor for aggregation-induced emission. Chem Commun 2007(3):231-3.

908 [80] Kwon OP, Ruiz B, Choubey A, Mutter L, Schneider A, Jazbinsek M, *et al.* Organic nonlinear
909 optical crystals based on configurationally locked polyene for melt growth. Chem Mater

2006;18(17):4049-54.

[81] Gainsford GJ, Ashraf M, Kay AJ. 2-{3-cyano-4-[2-(4-diethylamino-2-hydroxyphenyl)ethenyl]-5,5-dimethyl-2,5-dihydrofuran-2-ylidene}malononitrile acetone 0.25-solvate. Acta Crystallogr Sect Sect E: Struct Rep Online 2012;68(10):o2991-o2.

[82] Li S, Li M, Qin J, Tong M, Chen X, Liu T, *et al.* Synthesis, crystal structures and nonlinear optical properties of three tcf-based chromophores. CrystEngComm 2009;11(4):589-96.

[83] Khodorkovsky V, Mazor RA, Ellern A. 2-(p-diethylaminobenzylidene)-1,3-indandione. Acta Crystallogr Sect C: Cryst Struct Commun 1996;52(11):2878-80.

[84] Würthner F, Kaiser TE, Saha-Möller CR. J-aggregates: From serendipitous discovery to supramolecular engineering of functional dye materials. Angew Chem Int Ed 2011;50(15):3376-410.